CANCER

METTL6 is a tRNA m³C methyltransferase that regulates pluripotency and tumor cell growth

Valentina V. Ignatova[1], Steffen Kaiser[2]*, Jessica Sook Yuin Ho[3,4]*, Xinyang Bing[5]*, Paul Stolz[6], Ying Xim Tan[3], Chee Leng Lee[3], Florence Pik Hoon Gay[3], Palma Rico Lastres[1], Raffaele Gerlini[7,8], Birgit Rathkolb[7,8,9], Antonio Aguilar-Pimentel[7], Adrián Sanz-Moreno[7], Tanja Klein-Rodewald[7], Julia Calzada-Wack[7], Emil Ibragimov[1], Magdalena Valenta[1], Saulius Lukauskas[1], Andrea Pavesi[3], Susan Marschall[7], Stefanie Leuchtenberger[7], Helmut Fuchs[7], Valerie Gailus-Durner[7], Martin Hrabe de Angelis[7,8,10], Sebastian Bultmann[6], Oliver J. Rando[5], Ernesto Guccione[3,11], Stefanie M. Kellner[2], Robert Schneider[1,8,12]†

Recently, covalent modifications of RNA, such as methylation, have emerged as key regulators of all aspects of RNA biology and have been implicated in numerous diseases, for instance, cancer. Here, we undertook a combination of in vitro and in vivo screens to test 78 potential methyltransferases for their roles in hepatocellular carcinoma (HCC) cell proliferation. We identified methyltransferase-like protein 6 (METTL6) as a crucial regulator of tumor cell growth. We show that METTL6 is a bona fide transfer RNA (tRNA) methyltransferase, catalyzing the formation of 3-methylcytidine at C32 of specific serine tRNA isoacceptors. Deletion of *Mettl6* in mouse stem cells results in changes in ribosome occupancy and RNA levels, as well as impaired pluripotency. In mice, *Mettl6* knockout results in reduced energy expenditure. We reveal a previously unknown pathway in the maintenance of translation efficiency with a role in maintaining stem cell self-renewal, as well as impacting tumor cell growth profoundly.

INTRODUCTION

Similar to the well-established role for DNA and histone modifications in the control of gene expression (*1*, *2*), it is increasingly clear that the epitranscriptome—consisting of an ever-expanding set of covalent modifications to RNAs—is a crucial additional layer in gene regulation (*3*, *4*). There are currently more than 170 RNA modifications described in all classes of RNA (*5*). The resurgent interest in RNA modifications has been triggered by recent discoveries of novel types and sites of RNA modifications, of the specific enzymes that add or remove modifications, as well as of binding proteins (*6*). Many RNA-modifying enzymes and binding proteins have been implicated in different types of diseases and are thus novel targets for drug development (*7*–*10*).

Methylations are among the most prevalent RNA modifications. Different types of RNA methylations can be catalyzed by a large family of methyltransferase-like proteins (METTLs) that contain characterized as well as many predicted methyltransferases (*11*). Multiple METTL proteins have been implicated in different types of cancers

(*7*, *12*). METTL3, in a complex with its interaction partner METTL14 (*6*), catalyzes N6-methyladenosine (m⁶A) in mRNAs and noncoding RNAs (*13*) and can promote oncogene expression and cancer cell growth in leukemia (*14*). In addition, METTL14 and METTL3 play oncogenic roles in hepatocellular carcinomas (HCCs) (*7*). METTL1 up-regulation correlates with poor prognosis for patients with HCC and with HCC progression (*12*). It has been shown that METTL1 catalyzes 7-methylguanosine (m⁷G) formation in microRNAs (*15*) and transfer RNA (tRNAs) (*10*).

Modifications of tRNA can, for example, control tRNA stability, folding, decoding properties, or interactions with the translation machinery (*16*). tRNA modifications play key roles in the control of global protein synthesis rate, and an increasing number of cancer-causing mutations have been mapped to human genes that encode tRNA-modifying enzymes (*17*). Loss of the 5-methylcytidine (m⁵C) catalyzing tRNA methyltransferase NSun2 and of the pseudouridine synthase PUS7 was shown to promote tumorigenesis (*8*, *9*). Multiple enzymes involved in modifications of wobble uridine 34 in tRNAs have been implicated in resistance to targeted therapy and survival of melanoma cells (*18*). tRNA modifications and modifying enzymes were also shown to play crucial roles during cellular differentiation processes. For instance, Mettl1 is required for embryonic stem cell (ESC) self-renewal and differentiation toward neural lineages (*10*), PUS7 is required for germ layer specification (*9*), and NSun2 for differentiation of epidermal stem cell (*8*). Since tRNA modifications and protein synthesis rate have been linked with tumor progression and cellular differentiation, tRNA-modifying enzymes represent promising targets for drug discovery (*19*).

Despite the recent progress in the epitranscriptomics field and a clear medical relevance, the biological functions of most of the modified RNA nucleotides and the enzymes that catalyze these modifications remain to be discovered. Here, we demonstrate that METTL6 is a tRNA^Ser-specific 3-methylcytidine (m³C) methyltransferase and studied its functions. We found that METTL6 affects tumor cell growth

[1]Institute of Functional Epigenetics, Helmholtz Zentrum München, 85764 Neuherberg, Germany. [2]Chemical Faculty, Ludwig-Maximilians Universität München, Munich, Germany. [3]Institute of Molecular and Cell Biology (IMCB), Agency for Science, Technology and Research (A*STAR), Singapore, Singapore. [4]Department of Microbiology, Icahn School of Medicine at Mount Sinai, New York, NY 10029, USA. [5]University of Massachusetts Medical School, Worcester, MA 01605, USA. [6]Department of Biology II, Human Biology and Bioimaging, Ludwig-Maximilians Universität München, Munich, Germany. [7]German Mouse Clinic, Institute of Experimental Genetics, Helmholtz Zentrum München, 85764 Neuherberg, Germany. [8]German Center for Diabetes Research (DZD), 85764 Neuherberg, Germany. [9]Institute of Molecular Animal Breeding and Biotechnology, Gene Center, Ludwig-Maximilians-University München, Munich, Germany. [10]Chair of Experimental Genetics, School of Life Science Weihenstephan, Technische Universität München, 85354 Freising, Germany. [11]Mount Sinai Center for Therapeutics Discovery, Departments of Pharmacological Sciences and Oncological Sciences, Tisch Cancer Institute, Icahn School of Medicine at Mount Sinai, New York, NY 10029, USA. [12]Faculty of Biology, Ludwig-Maximilians Universität München, Munich, Germany.
*These authors contributed equally to this work.
†Corresponding author. Email: robert.schneider@helmholtz-muenchen.de

both in vitro and in a mouse xenograft model. In mouse ESCs (mESCs), loss of METTL6 has widespread effects on mRNA levels and on translation. Depletion of METTL6 results in defects in cellular growth and compromised pluripotency. METTL6 knockout (KO) mice display metabolic phenotypes that manifest itself in reduced energy turnover. These findings reveal METTL6-mediated m^3C tRNA methylation as a novel regulatory mechanism of gene expression, translation, cell homeostasis, and tumor cell growth.

RESULTS

METTL6 KD reduces growth rate of tumor cells

To systematically investigate the role of members of the extended methyltransferase family in tumor cell proliferation, we designed an in vivo and in vitro methyltransferase-centric pooled lentiviral short hairpin RNA (shRNA) screen. The screen comprised 506 unique shRNAs against mRNAs encoding 78 potential methyltransferases from the PRMT (protein arginine methyltransferase), PRDM (RDI-BF1 and RIZ homology domain containing), NSUN (Nol1/Nop2/SUN domain), and METTL protein families (table S1A), as well as MYC as a positive control. We used three to five shRNAs per target mRNA (table S1A), packaged the shRNA library pool into lentivirus particles, and infected the human HepG2 HCC cell line. We chose this cell line because these cells do not contain known mutations in any of our target genes (20) and are easy to manipulate in both in vitro cell culture and in vivo xenograft experiments. We cultured the shRNA-expressing cells either in vitro or injected subcutaneously them in the flanks of CB17-SCID (severe combined immunodeficient) mice to allow tumor formation (Fig. 1A). This screen was conducted in two biological replicates. We hypothesized that shRNAs targeting genes that are essential for growth or required to maintain oncogenic programs would be lost, whereas shRNAs targeting genes with tumor-suppressive functions would be enriched over time.

As expected, multidimensional scaling plots revealed that shRNAs recovered from in vivo tumors and in vitro passaged cells clustered more closely to each other compared to the initial viral and plasmid inputs. Over time, hairpin abundances changed (fig. S1A) and most hairpins that were depleted in the in vitro passaged cells were also depleted in in vivo tumors. The same was also true for enriched hairpins (fig. S1B and table S1, B and C).

To identify genes that were important for in vitro and in vivo cell growth, we performed a rotational gene set analysis (21) of our pooled screen data (table S1, D and E). This revealed 34 genes for which the abundance of their targeting hairpins significantly changed in vitro (Fig. 1B and table S1D) and 17 genes whose targeting hairpins significantly changed abundance in vivo (Fig. 1B and table S1E). As expected, the positive control shRNAs targeting *MYC* mRNA were depleted in both the in vivo and in vitro datasets (Fig. 1B, top). Seven other genes, including three METTL proteins (METTL6, FBL, KIAA1627, METTL13, C1of156, METTL7B, and PRDM5), were also represented in both datasets and are thus important for maintaining cell growth both in vitro and in vivo. Of these seven genes, METTL6 was the most significant hit shared between the two datasets (Fig. 1B), suggesting that METTL6 supports tumor cell growth in vitro and in vivo.

Next, we wanted to investigate the consequences of METTL6 depletion in HepG2 cells in more detail by using individual shRNAs (fig. S1, C and D). We observed a reduction in growth rate upon depletion of METTL6 (Fig. 2A). Cell cycle analysis of METTL6 knock-

down cells showed a tendency toward increased accumulation at the G_1 phase of cell cycle (fig. S1E), with a reduced entry into S phase (Fig. 2B) when compared to scrambled shRNA-treated cells. We did not detect a marked increase in the percentage of apoptotic cells or accumulation of cells in G_2 phase (fig. S1E). In addition, METTL6 depletion in HepG2 impaired anchorage-independent growth (Fig. 2C and fig. S1F) and reduced colony formation capacity (Fig. 2D and fig. S1G). These data point toward a reduced tumorigenic potential of METTL6 knockdown cells, supporting our xenograft studies (Fig. 1, A and B). We lastly reanalyzed the TCGA (The Cancer Genome Atlas) HCC dataset, to assess any correlation between *METTL6* mRNA expression and differential patient survival rates. Consistent with a pro-proliferative function of METTL6, patients with low *METTL6* levels have increased survival rates (Fig. 2E). We, therefore, decided to study METTL6 further to gain insight into its activity and mechanistic function.

METTL6 methylates tRNAs in vitro

METTL6 was predicted to be a homolog of the *Saccharomyces cerevisiae* tRNA methyltransferase Trmt140 (22); however, experimental confirmation of its direct catalytic activity has, so far, been missing (22). We therefore investigated whether recombinant human METTL6 has RNA methyltransferase activity. Thus, we expressed and purified glutathione *S*-transferase (GST)–tagged METTL6 (fig. S2, A and B) and used it in in vitro methyltransferase assays on total RNA, isolated from HeLa cells, with tritium-labeled *S*-adenosyl methionine (SAM) as methyl group donor. As shown in Fig. 3A, GST-METTL6 methylated total RNA; however, mutations of METTL6 at N92 or F111, two key residues within the SAM-binding region, abolished the activity.

To identify the type of methylation catalyzed by METTL6, we applied Methyl–NAIL (nucleic acid isotope labeling)–MS (mass spectrometry) (23) as an unbiased approach. For this, we grew cells in medium containing CD_3-methionine for 7 days to ensure that all methyl groups in the cells contain deuterium. We then isolated RNA from these cells for in vitro RNA methyltransferase assays with recombinant GST-METTL6 and unlabeled SAM as methyl group donor. This allowed us to exploit the mass difference between metabolically inserted deuterium containing methylated nucleosides and unlabeled methylated nucleosides that were methylated in vitro by METTL6 (Fig. 3B and table S2). Using liquid chromatography–tandem MS (LC-MS/MS), we identified m^3C as the nucleoside de novo methylated by METTL6. We did not observe de novo formation of m^5C or m^3U, demonstrating that human METTL6 is an m^3C methyltransferase (Fig. 3B).

Having shown that METTL6 itself can methylate cytidine at position 3, we next wanted to investigate systematically which RNA species become methylated. For this, we size-fractionated the in vitro methylated RNA from the Methyl-NAIL experiment. We detected a strong (>15-fold) increase in the m^3C levels in the tRNA-containing fraction (Fig. 3C). This effect is specific for m^3C as we did not detect noticeable alterations in the levels of other types of methylations analyzed (Fig. 3D and fig. S2C), demonstrating that METTL6 catalyzes m^3C in tRNAs.

Comparative NAIL-MS demonstrates that METTL6 methylates specific tRNA[Ser] isoacceptors in cells

To confirm the activity and specificity of METTL6 in cells, we made use of human wild-type (WT) and METTL6 KO Haploid 1 (HAP1) cells [derived from the male chronic myelogenous leukemia cell line
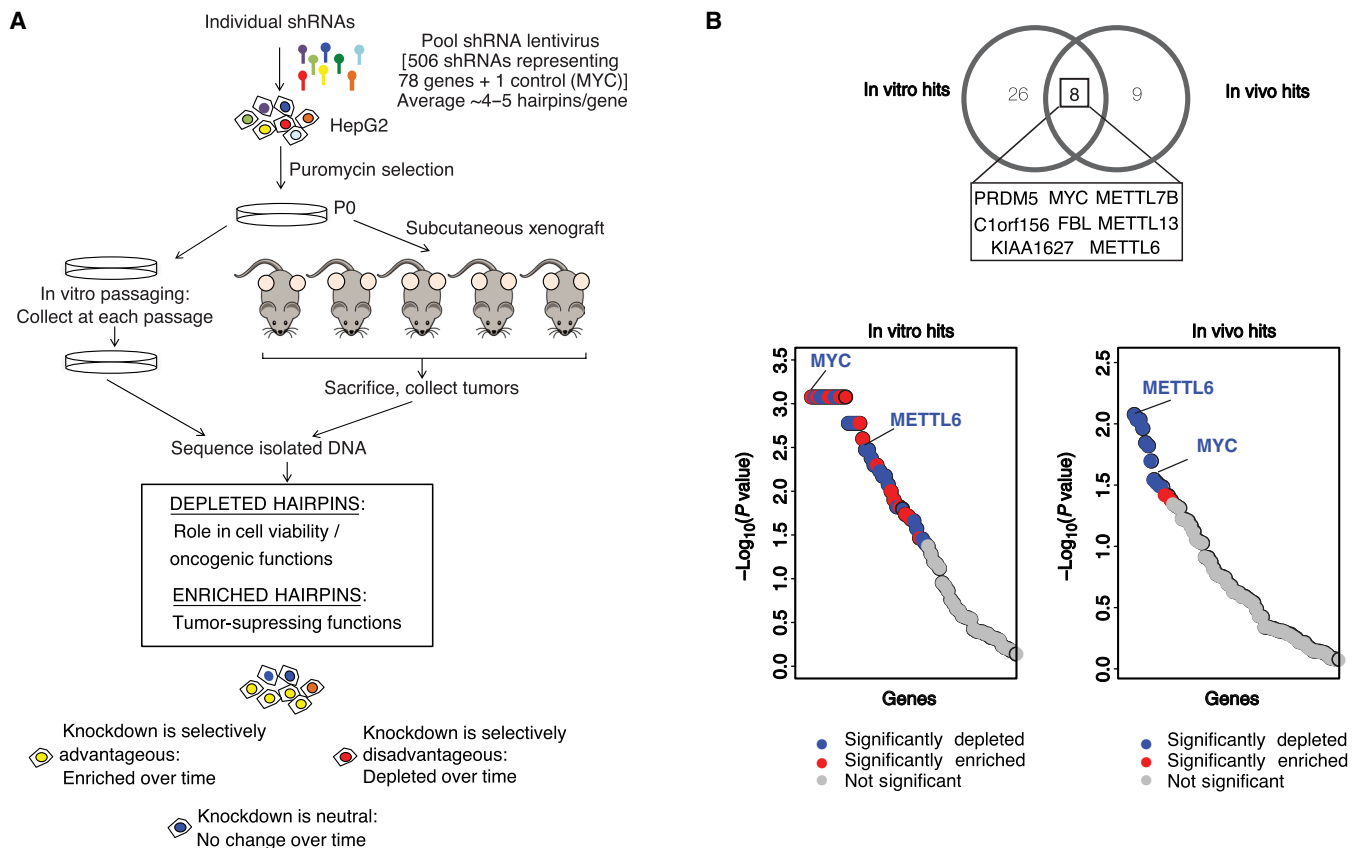
Fig. 1. METTL6 is important for HCC cell growth. (**A**) Scheme of the setup of pooled shRNA screen. HepG2 cells were infected with viruses carrying 506 shRNAs targeting 78 members of the methyltransferase family and MYC as control. The cells were in vitro passaged (left) or injected into mice (right). After isolation of DNA, the depletion or enrichment of shRNAs was determined by sequencing (see Materials and Methods for details). (**B**) Top: Venn diagram showing the overlap of in vivo and in vitro screen hits. Bottom left: Rotation gene set testing (ROAST) of the significantly [$P < 0.05$; false discovery rate (FDR) < 0.26] depleted (blue dots) and enriched (red dots) shRNA hairpins in tumor cells isolated from mice. Genes were sorted by their ROAST P values. Ranks of both METTL6 and MYC (positive control) are indicated. Bottom right: Rotational gene set analysis of the significantly ($P < 0.05$; FDR < 0.05) depleted (blue dots) and enriched (red dots) shRNA hairpins in the in vitro passaged cells. Genes are sorted by their ROAST P values. Ranks of both METTL6 and MYC are indicated. For a full list of genes, see table S1.

KBM-7 (*24*)]. Consistent with our in vitro studies, RNA isolated from these KO cells exhibited decreased m^3C levels compared to RNA from wt cells (Fig. 4A and fig. S2D). Next, we analyzed m^3C levels in different gel-purified tRNA factions, isolated from the METTL6 KO and wt cells (fig. S2E). Upon loss of METTL6, we did not detect significant alterations in the m^3C levels in the tRNA fraction with a length of 70 to 80 nucleotides (nt). However, we found strongly reduced levels of m^3C in the tRNA fraction of approximately 85 nt (Fig. 4B, fig. S2E, and table S2). These 85-nt fractions contain type II tRNAs with a long variable loop extension: serine tRNAs (tRNA^{Ser}) and leucine tRNA (tRNA^{Leu}) (*25*), limiting the in vivo targets for METTL6 to serine and leucine tRNAs and their isoacceptors.

To profile tRNA isoacceptors for the presence of m^3C, we isolated isoacceptors by hybridization with specific DNA probes (fig. S2F and table S2) (*26*) and subsequently analyzed the modification content per isoacceptor (isolated from wt and METTL6 KO cells) by isotope dilution MS. To avoid biases, for example, due to variations in the efficiency of tRNA purifications, we chose to apply comparative NAIL-MS. For this, we grew METTL6 KO cells in $^{13}C_6$-glucose–containing medium (supplemented with unlabeled adenine) and wt cells in unlabeled medium, combined both cell types, and purified

tRNA isoacceptors. This resulted in one major heavy isotopomer for each nucleoside with a mass increase of +5 (derived from $^{13}C_5$-ribose) from cells grown in labeled medium compared to nucleosides from unlabeled medium. Thus, we were able to distinguish tRNAs from wt and METTL6 KO cells as well as to perform absolute quantification of modifications. In the tRNA isoacceptors from wt cells, we detected approximately one molecule of m^3C in the serine isoacceptors tRNA$^{Ser}_{CGA}$, tRNA$^{Ser}_{GCU}$, and tRNA$^{Ser}_{UGA/AGA}$ as well as in the arginine isoacceptors tRNA$^{Arg}_{UCU}$ and tRNA$^{Arg}_{CCU}$ and in the threonine isoacceptors tRNA$^{Thr}_{CGU}$ and tRNA$^{Thr}_{UGU}$. For tRNA$^{Ser}_{ACU}$ and tRNA$^{Thr}_{AGU}$, we found only half of this amount (Fig. 4C, black; fig. S2G; and table S2). The presence of m^3C in these tRNA isoacceptors is consistent with previous sequencing-based assays that suggested that m^3C occurs at positions 32 and/or 47d of several serine and threonine tRNA isoacceptors as well as two arginine tRNA isoacceptors (*27*). Upon loss of METTL6, we observed an approximately twofold decrease of m^3C levels in the tRNA$^{Ser}_{CGA}$, tRNA$^{Ser}_{GCU}$, and tRNA$^{Ser}_{UGA/AGA}$ isoacceptors (Fig. 4C, red), suggesting a loss of one methylation site. In contrast to this, we observed no effect on the m^3C levels in arginine and threonine tRNAs. Of note, the levels of another prominent tRNA modification, m^5C, were not affected by the METTL6
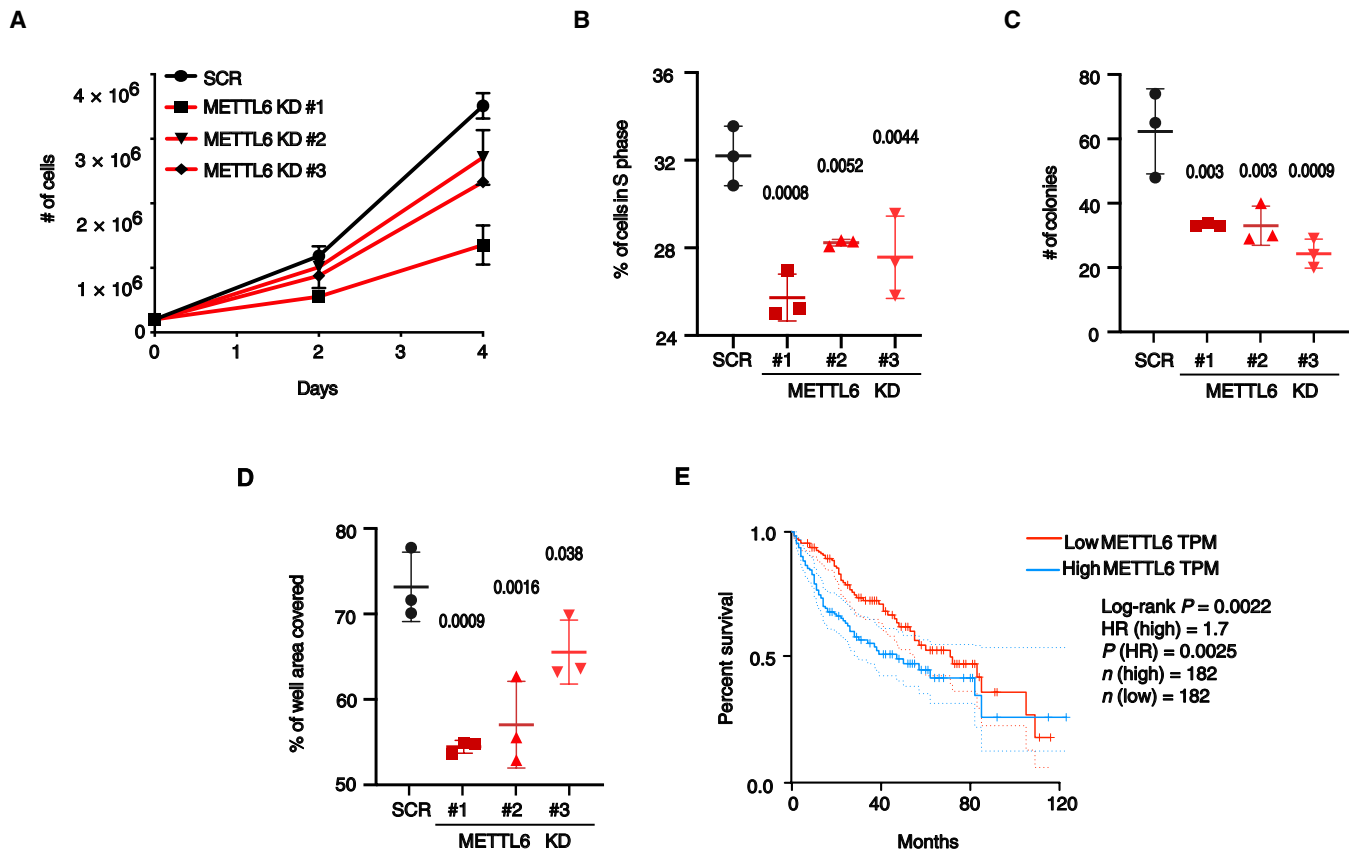
Fig. 2. Loss of METTL6 affects HepG2 growth and colony formation. (**A**) Growth curves of HepG2 cells infected with either control (SCR) or METTL6 targeting shRNAs. Average cell number of two technical replicates and SD are plotted. Representative experiment of three independent experiments. (**B**) Percentage of HepG2 cells (SCR or METTL6 shRNAs) in S phase 2 days after selection analyzed by flow cytometry. Average of triplicate wells and individual data points are shown. Error bars: SD. *P* values: one-way analysis of variance (ANOVA) followed by Holm-Sidak's post hoc test compared to controls. (**C**) Quantification of colonies formed by HepG2 cells (SCR or METTL6 shRNAs) in soft agar. Average of triplicate wells as well as individual data points. Error bars and *P* values are as in (B). (**D**) Colony formation assay of HepG2 cells (SCR or METTL6 shRNAs). Average of percentage of well area occupied by cells in triplicate wells as well as individual data points. Error bars: SD of three experimental replicates, *P* values as in (B). (**E**) Overall survival curves of patients with high (blue) or low (red) METTL6 mRNA levels. Data were obtained from publicly available The Cancer Genome Atlas datasets for HCC and plotted using GEPIA (Gene Expression Profiling Interactive Analysis) (*55–57*). Log-rank *P* value and hazard ratios (HR) are indicated.

KO (fig. S2H). Together, this demonstrates that METTL6 methylates specific tRNA^{Ser} isoacceptors, but not tRNA^{Thr} in vivo.

To demonstrate that serine tRNAs are indeed a direct METTL6 target and to map the methylated cytosine within the tRNA^{Ser} isoacceptors, we used in vitro transcribed tRNA$^{Ser}_{UGA}$ (*28*) wt or with C32-to-G and C47d-to-U mutations as substrates in in vitro RNA methyltransferase assays with recombinant GST-METTL6 and tritium-labeled SAM as methyl group donor. As shown in Fig. 4D, mutation of C32 but not C47 in tRNA$^{Ser}_{UGA}$ abolished methylation by METTL6. Thus, our data demonstrate that METTL6 is, by itself, a methyltransferase that targets specific tRNA^{Ser} isoacceptors.

Loss of METTL6 affects gene expression and ribosome occupancy

Next, we wanted to decipher molecular consequences of METTL6 loss in a cell culture model. As HAP1 cells are an unstable haploid cell line that can spontaneously diploidize, we decided to generate *Mettl6* KO mESCs as a more suitable biological model for further analysis (fig. S3, A and B). As expected, we observed a >2-fold drop in the m^{3}C levels in the tRNA fraction of approximately 85 nt isolated from these *Mettl6* KO mESCs (fig. S3C). Transient expression of wt

METTL6, but not an N92 mutant, partially rescued m^{3}C levels and had, as expected, no effect on m^{5}C levels (fig. S3C). This validates *Mettl6* KO mESCs as a suitable model to study METTL6 function in nontransformed cells. To investigate the effects of m^{3}C tRNA^{Ser} methylation on translation, we carried out transcriptome-wide ribosome profiling (*29*, *30*). In order to calculate translation efficiency per gene, we combined ribosome profiling in these *Mettl6* KO and wt mESCs with RNA abundance profiling (fig. S3D; see table S3 for data).

Focusing on gene-level changes in transcript abundance and ribosome occupancy, we identified several hundred transcripts with significantly altered ribosome occupancy [adjusted *P* < 0.05, log$_2$ fold change (FC) > 0.5] in *Mettl6* KO mESCs relative to the paired wt control (approx. 500 transcripts with decreased and approx. 700 transcripts with increased ribosome occupancy) (Fig. 5A). In agreement with multiple prior ribosome footprinting analyses of tRNA modification mutants (*30–33*), most of the changes in ribosome occupancy resulted from altered mRNA abundance, potentially reflecting secondary effects of a changed biological state of *Mettl6* KO cells. Thus, most of the changes that we observed could represent widespread regulatory derangements caused by upstream changes. We found that transcripts exhibiting significant ribosome occupancy
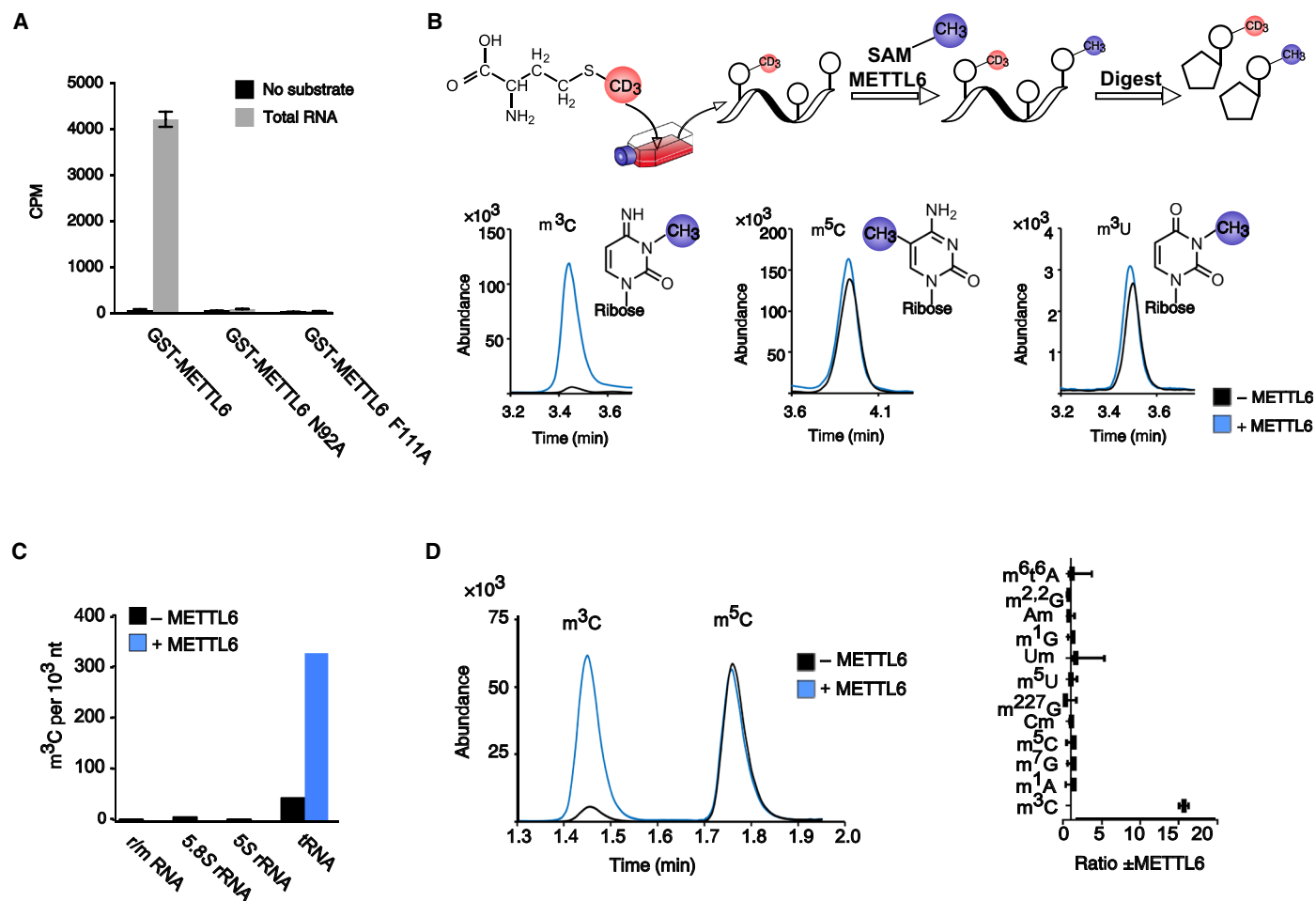
Fig. 3. METTL6 catalyzes m³C in tRNAs in vitro. (A) In vitro methyltransferase assay on HeLa total RNA with recombinant (wt) GST-METTL6 and GST-METTL6 N92 to A and F111 to A mutants and tritium-labeled SAM. Tritium signal was quantified by liquid scintillation counting. Counts per minute (CPM) of three replicates; error bars reflect SD. **(B)** Top: Principle of Methyl-NAIL-MS (*23*). For details, see the main text. Methylated nucleosides were analyzed by LC-MS/MS. Bottom: Overlaid MS/MS chromatograms of CH₃ and CD₃-labeled m³C, m⁵C, and 3-methyluridine (m³U). Incubation with SAM and METTL6 (blue) increased the abundance of m³C, compared to incubation with SAM alone (black). **(C)** Fractionation of total RNA from (B) using size exclusion chromatography and quantification of m³C abundance. Main components of fractions: (i) large ribosomal RNAs (rRNAs) and mRNA, (ii) 5.8*S* rRNA, (iii) 5*S* rRNA, and (iv) tRNAs. Number of m³C per 1000 nt of samples incubated with SAM and GST-METTL6 (blue) or SAM only (black) is plotted. **(D)** Left: LC-MS/MS chromatogram showing abundance of m³C and m⁵C in the tRNA fraction after incubation with SAM (black) or SAM and METTL6 (blue). Right: Ratio of r/m RNA, Ribosomal/Messenger RNA. modifications after incubation with METTL6 and SAM versus incubation with no enzyme determined by LC-MS/MS (average of three replicates; error bars reflect SD).

changes in *Mettl6* KO mESCs are involved in a number of biological processes (Fig. 5B), including proliferation-related genes as reflected in decreased ribosome occupancy at transcripts of cell cycle genes, RNA-binding proteins, and core histone genes, along with increased ribosome occupancy at transcripts of genes related to signaling, development, and growth control (*Notch1*, *Notch2*, *Fgf4*, *Egfr*, *Pdgfa*, *Nodal*, *Fgfr2*, etc.). Translation and proteostasis were also broadly affected by the loss of *Mettl6* as evidenced by the broad alteration of transcripts involved in ribosome biogenesis, translation (*Gtf2e2*, *Eif5a*, *Eif4a1*, *Eif2a1/2*, *Eif3m*, *Rps6ka6*, etc.), tRNA aminoacylation (e.g., *Kars*, *Gars*, *Aars*, *Lars*, and *Nars*), and proteasome assembly (*Psmd12*, *Psma4*, *Psmd11*, *Psmb6*, *Psmb3*, *Psmd13*, *Psmd1*, etc.).

Mettl6 loss in mESCs affects pluripotency

Next, we addressed whether the mis-regulation on the mRNA and translation levels upon METTL6 loss affects mESCs stemness. For

this, we analyzed self-renewal and pluripotency of *Mettl6* KO mESCs grown under standard serum–leukemia inhibitory factor (LIF) conditions. Under these conditions, we observed morphological changes in *Mettl6* KO with a decrease in the number of round, compact ESC colonies and a concomitant increase of rather flat, differentiated-looking cells (Fig. 6A). This is in line with our alkaline phosphatase (AP) staining where we observed a clear loss of AP-positive pluripotent cells after 5 days, suggesting a tendency to differentiate and reduced self-renewal (Fig. 6B). To obtain a broader view of potential changes in gene expression upon *Mettl6* loss, we performed RNA sequencing (RNA-seq) of cells grown in serum-LIF (fig. S4A). Consistent with the increased differentiation of *Mettl6* KO cells, we observed a reduction in the RNA levels of the pluripotency factors, in particular of those transcription factors associated with naïve pluripotency such as *Zfp42* (*Rex1*), *Klf4*, *Esrrb*, *Tbx3*, and *Dppa3* and of signaling pathway genes such as *Lifr* (Fig. 6C and table S4). Although
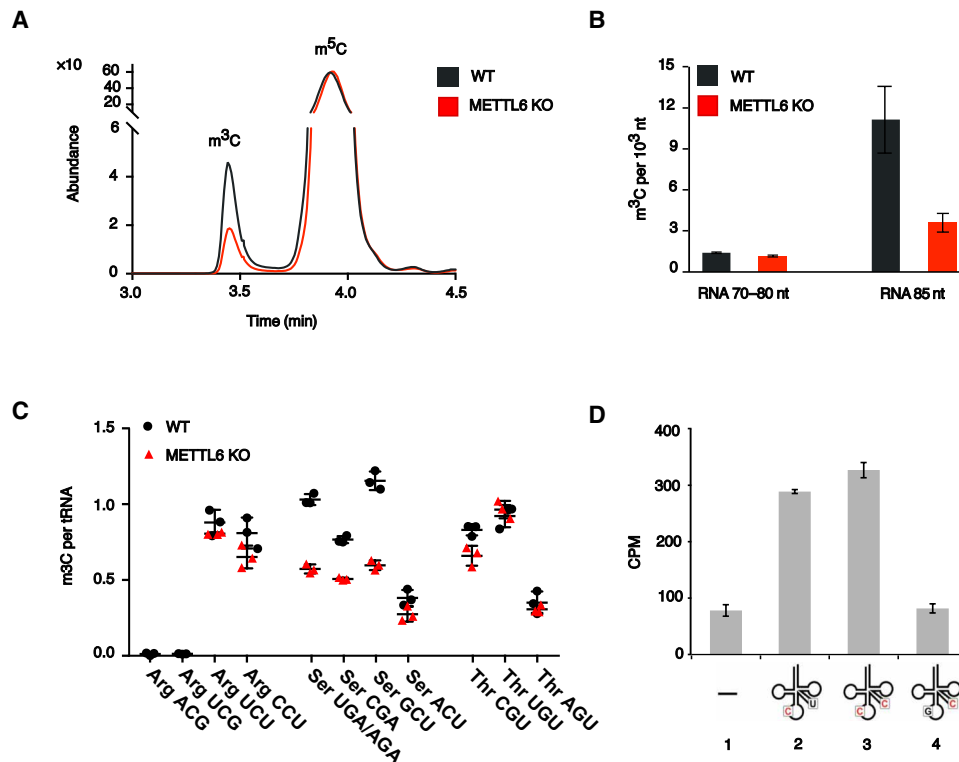
Fig. 4. METTL6 methylates specific serine tRNAs in cells. (**A**) LC-MS/MS chromatogram of total RNA from wt (black) and METTL6 KO (red) HAP1 cells. Chromatogram of mass transition from 258 to 126 is shown. The first peak is identified as m^{3}C and the second is identified as m^{5}C using synthetic standards. The retention times are provided in table S2. (**B**) LC-MS/MS analysis of HAP1 tRNA of 70 to 80 nt length and 85 nt length from wt (black) and METTL6 KO (red). Note the drop in m^{3}C per 1000 nt in the tRNA fraction of 85 nt (average of three biological replicates shown; error bars reflect SD). (**C**) Comparative NAIL-MS for comparison of m^{3}C abundance in tRNA isoacceptors purified from wt (black) and METTL6 KO HAP1 cells (red). Only specific tRNA serine isoacceptors (tRNA$^{Ser}_{CGA}$, tRNA$^{Ser}_{GCU}$, and tRNA$^{Ser}_{UGA/AGA}$ show a decrease in m^{3}C abundance upon loss of METTL6, while tRNA threonine and arginine isoacceptors are not affected. Note that we cannot distinguish between tRNA$^{Ser}_{UGA}$ and tRNA$^{Ser}_{AGA}$. (**D**) In vitro RNA methyltransferase assay on in vitro transcribed wt tRNA$^{Ser}_{UGA}$ and C47d-to-U and C32-to-G mutants with recombinant wt GST-METTL6 (performed as in Fig. 3A). Note that C32 is the target for METTL6.

Pouf5f1/Oct4 was unchanged, these data indicate a general tendency toward pluripotency loss in the absence of *Mettl6* and an exit toward differentiation. In agreement with this, we noticed an up-regulation of gastrulation markers such as *Fgf5*, *Lefty1*, and *Nodal*, as well as of the mesoderm marker *Brachyury* (*T*) and the ectoderm marker *Nestin* (*Nes*) (Fig. 6C and table S4). We observed that *Mettl6* KO mESCs consistently have lower number of cells during passaging and quantified this by growth curves (Fig. 6D). To investigate potential underlying causes, we performed cell cycle and apoptosis analyses. We found that the percentage of early apoptotic cells in *Mettl6* KO mESCs was approximately double compared to wt mESCs (Fig. 6E), without obvious changes in cell cycle (fig. S4B). In agreement with this, we detected 86 genes associated with the Gene Ontology (GO) term "positive regulation of apoptotic process" to be up-regulated upon *Mettl6* KO (including *Bbc3*, *Unc5b*, *Lats2*, *Pmaip1*, and *Bcl2l11*) in our RNA-seq analysis.

To further investigate the loss of pluripotency in *Mettl6* KO mESC, we assayed embryoid body (EB) formation (Fig. 6F). The *Mettl6* KO cells initially aggregated into EBs but later on formed vesicle-like structures and less organized tissues (fig. S4C). We analyzed the expression of the lineage markers *Brachyury* (*T*) (mesoderm), *Sox17* (endoderm), *Sox1* (neuroectoderm), and *Gata6* (primitive endoderm), as well as the pluripotency factors *Nanog* and *Sox2* after 8 days of EB differentiation. *Mettl6* KO EBs exhibited increased *Sox17* and *Gata6*

expression but showed a significant reduction in the mRNA levels of *Brachyury* and *Sox1* (Fig. 6G) as well as of *Nanog* and *Sox2*. This suggests that *Mettl6* KO mESCs exhibit an impaired differentiation potential skewed toward endodermal lineages and an impaired ability to activate neuroectodermal and mesodermal programs, indicative of reduced pluripotency. Together, these data suggest that loss of *Mettl6* in mESCs cells results in a compromised self-renewal and pluripotency potential as well as a skewed lineage commitment.

Mettl6 deficiency in mice leads to decreased metabolic activity

Next, to investigate the function of METTL6 in vivo, we generated *Mettl6*$^{-/-}$ mice. Homozygous KO mice were born at the expected Mendelian ratios (fig. S5A), indicating that *Mettl6* deficiency does not cause embryonic lethality. Systemic phenotyping revealed that adult *Mettl6* KO mice did not display overt morphological defects. However, male KO mice showed a significant reduction in body weight over time when compared to wt control animals ($P = 0.042$; random intercept and slope model) (Fig. 7A). When tested for glucose tolerance (GTT), 13-week-old KO mice showed an impaired glucose response (Fig. 7B). Fasting glucose levels were not altered, and after 120 min, glycemia returned to levels similar to those of control mice, pointing toward a delayed but functional response to a glucose bolus injection. Together, these data suggest a metabolic phenotype in *Mettl6* KO mice.
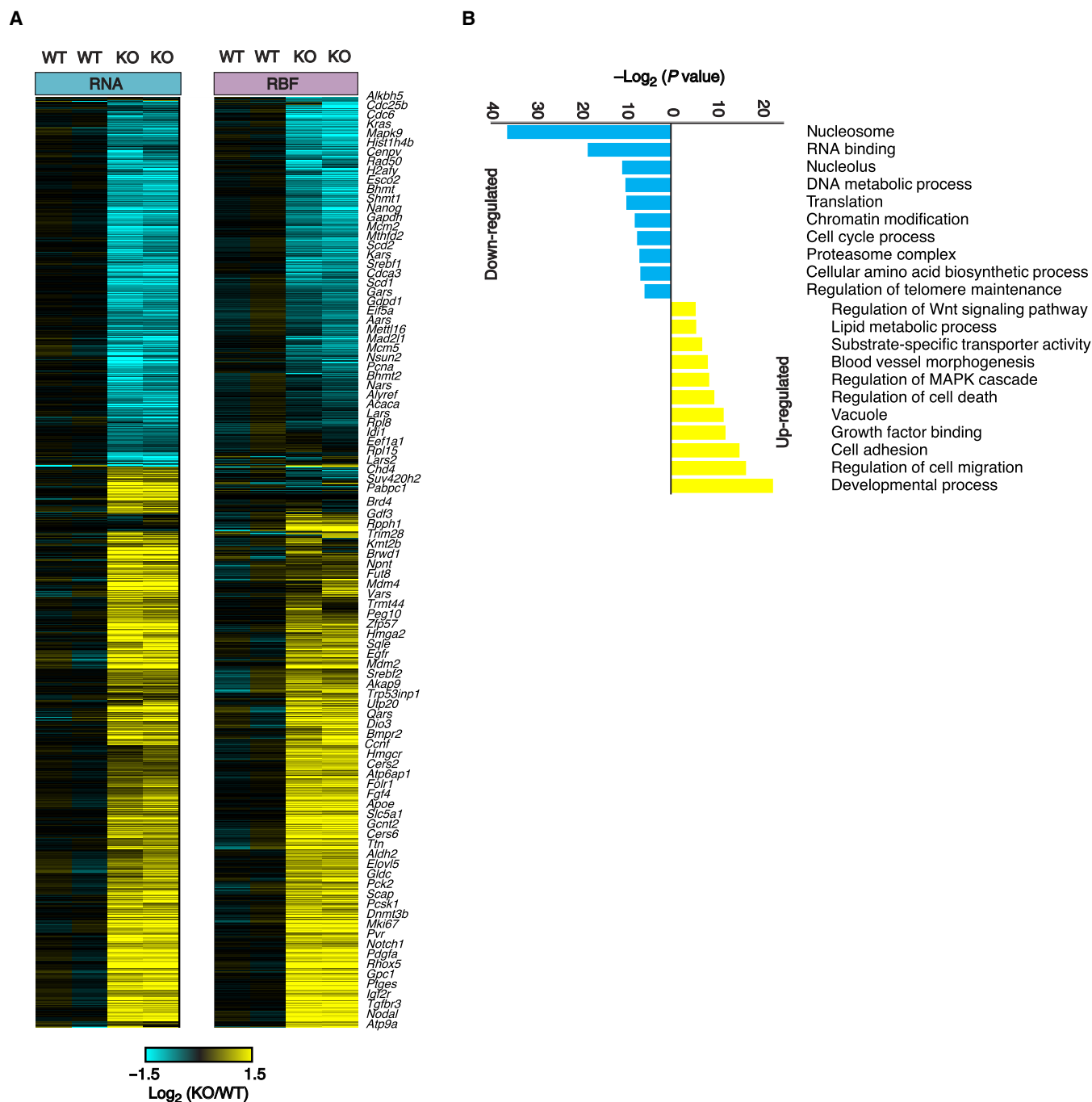
Fig. 5. Loss of m³C in tRNA^Ser affects mRNA translation. (**A**) Genome-wide changes in mRNA abundance and ribosome occupancy in wt and *Mettl6* KO. Heatmaps display changes in mRNA abundance (left) or ribosome occupancy (right) for two biological replicates of *Mettl6* KO and matched wt control, expressed as log₂ FC relative to the wt average. Genes exhibiting significant KO effects [DESeq *P* value of <0.05 (multiple hypotheses corrected)] on either RNA abundance (RNA) or ribosome occupancy (RBF) are shown. Names of selected genes are indicated. See also table S3. (**B**) Gene Ontology (GO) analysis of genes exhibiting significant ribosome occupancy changes in the METTL6 KO. Selected GO terms are shown, along with the −log₁₀ of the *P* value for their enrichment.

To investigate this phenotype further, we analyzed energy expenditure and oxygen consumption. *Mettl6* KO mice had reduced energy expenditure with decreased oxygen consumption (Fig. 7C). The diminished respiratory exchange rate (Fig. 7D) suggests that *Mettl6* KO mice use lipids over carbohydrates during the dark and active day phases, in which carbohydrate utilization is normally favored, despite comparable food intake. The reduction in heat production during the trial suggested a lower metabolic rate (Fig. 7E). While these differences were constant in males through light and dark cycles, females had lower metabolic rates in the dark and/or early light, but not in the late light phase (fig. S5, B to G). In line with the metabolic phenotype, livers of *Mettl6* KO mice weighed significantly less than in control animals (fig. S6A) (*P* = 0.009; linear model with body weight as covariate). In the absence of hepatic
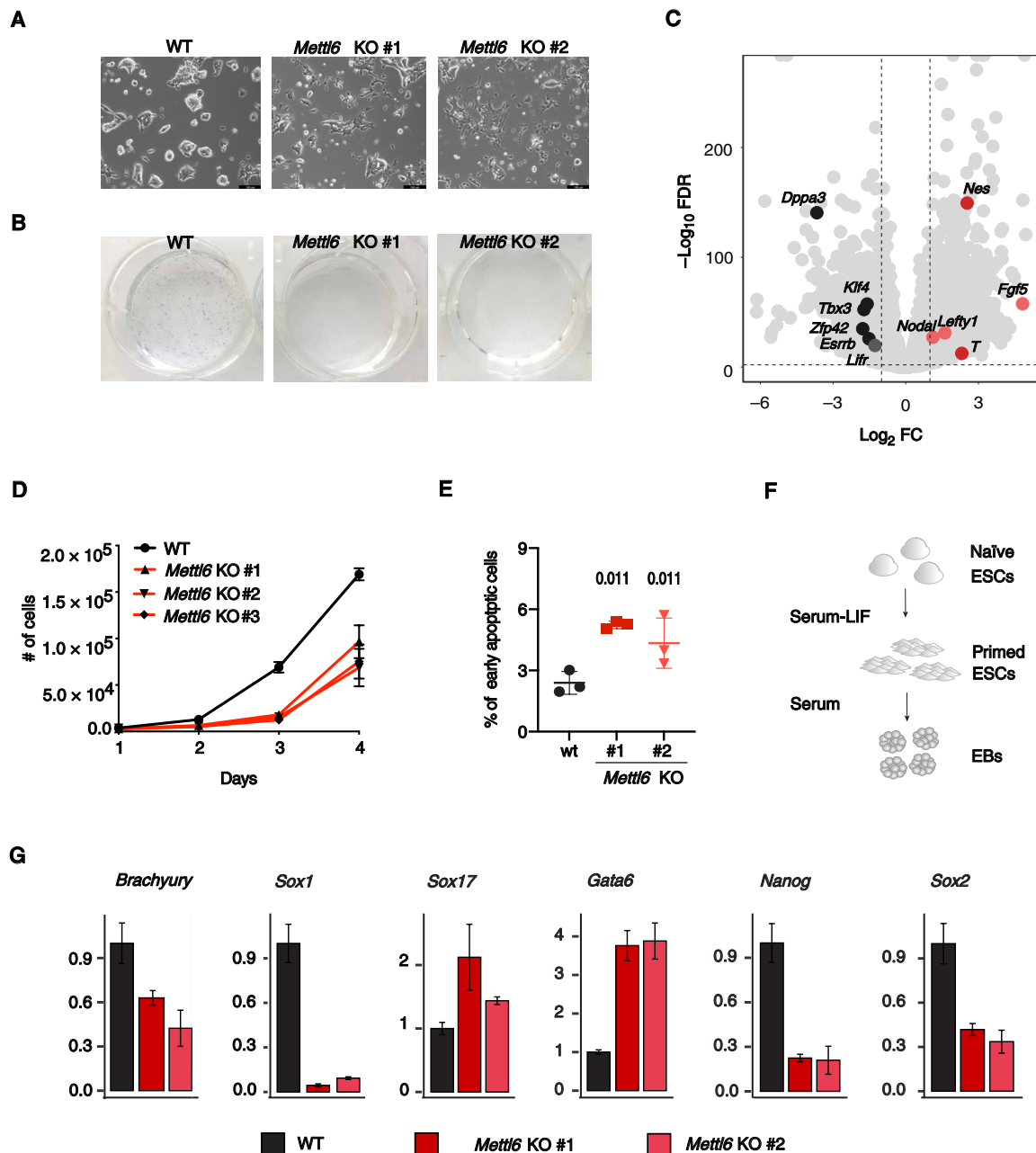
Fig. 6. *Mettl6* KO affects pluripotency in mESCs. (A) Bright-field cell images of wt and *Mettl6* KO mESCs 6 days in serum-LIF. Two fields from a representative experiment are shown. **(B)** AP staining of wt and *Mettl6* KO mESCs. Representative images of three independent experiments is shown. Photo credit: Paul Stolz, LMU. **(C)** Genes differentially expressed in *Mettl6* KO compared to wt mESCs. Pluripotency and lineage markers are in black and red. For full data, see table S4. **(D)** In vitro growth curves of wt and *Mettl6* KO mESCs. Representative experiment of two independent biological replicates. Number of cells averaged from eight technical replicates and SD are shown. **(E)** Percentage of early apoptotic cells in wt and *Mettl6* KO mESCs analyzed by annexin V staining. Data of three independent experiments are plotted. Error bars represent SD. *P* values are from paired *t* test. **(F)** Schematic representation of EB formation assay. **(G)** Reverse transcription quantitative polymerase chain reaction (RT-qPCR) analysis of expression levels of marker genes in wt (black) and *Mettl6* KO mESCs (red) at day 8 of EB assay. FCs quantified (RQ) relative to wt are plotted. Error bars indicate the SE on the average RQ (Relative Quantification) values of three replicates.

morphological alterations (fig. S5B), plasma activities of liver alanine aminotransferase (fig. S6C) and AP were lower in *Mettl6* KO animals (fig. S6D), suggesting that the changes in the metabolic activity upon *Mettl6* loss may not simply be due to hepatocellular damage in these animals. Together, these results reveal that *Mettl6* deficiency can result in a reduced energy turnover and altered substrate utilization linking m3C tRNA modification with metabolic regulation in an animal model.

DISCUSSION

Covalent modifications of tRNAs play a major role in their functionality (*3*) and have important roles in human pathologies (*34*). By using a combination of in vitro and in vivo approaches including comparative NAIL-MS, we identified METTL6 as a tRNA methyltransferase that specifically catalyzes m3C formation in distinct tRNA^{Ser} isoacceptors. We demonstrate the impact of *Mettl6* loss in
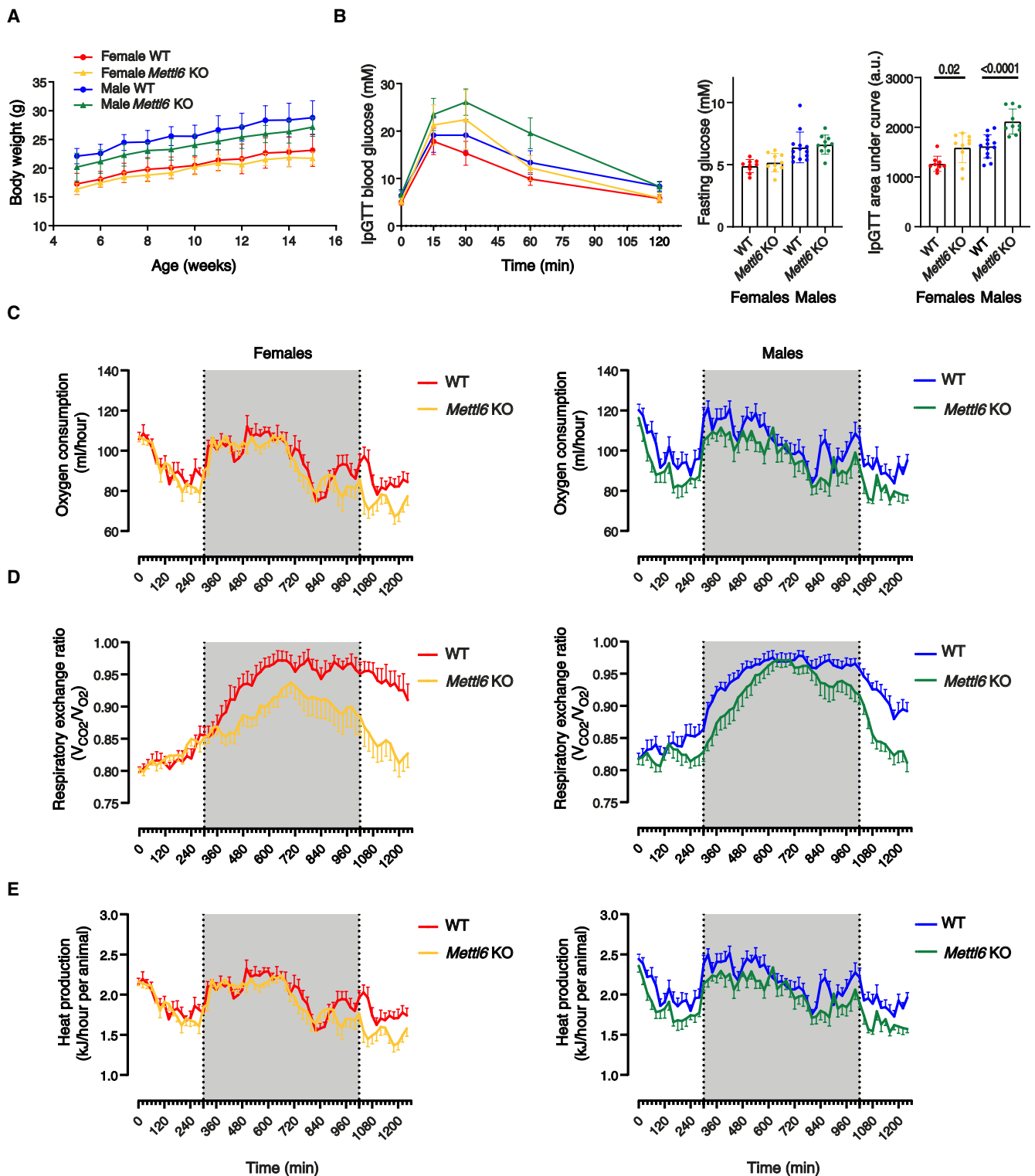
Fig. 7. Mettl6 KO mice have altered metabolic activity. (**A**) Body mass of *Mettl6* KO female and male mice and age-matched controls (wt) from 3 to 15 weeks (*n* = 11 to 15 per group). (**B**) Blood glucose curves during intraperitoneal glucose tolerance test (IpGTT). Blood glucose level was determined before (T0) and 15, 30, 60, and 120 min after intraperitoneal glucose administration in male and female *Mettl6* KO and age-matched wt mice (*n* = 9 to 13 per group). Basal fasting glucose level after overnight fasting at T0 before glucose injection (left) and area under the glucose curve above basal glucose level calculated according to trapezoidal approximation (right). a.u., arbitrary units. (**C** to **E**) Oxygen consumption (C), respiratory exchange ratio (D), and heat productions (E) in females (left) and males (right) measured every 20 min for 21 hours starting from the second half of the light phase (0 to 280 min) to the first half of the light phase (1040 to 1240 min) through the dark cycle (300 to 1020 min, gray zone). Data are represented as means ± SEM (*n* = 9 WT and *n* = 10 *Mettl6* KO in female group; *n* = 13 WT and *n* = 10 *Mettl6* KO in male group).

cellular models. Furthermore, by generating *Mettl6* KO mice, we identified the biological consequences of *Mettl6* loss in a full organism.

m^{3}C in tRNA^{Ser} is evolutionary conserved and has been identified in *S. cerevisiae* and *Saccharomyces pombe*. In *S. cerevisiae*, Trm140 and Trm141 catalyze m^{3}C formation in tRNA^{Thr} and tRNA^{Ser}, respectively (*35*, *36*). In mammals, there are three Trm140 and Trm141 homologs for which m^{3}C activity has been proposed: METTL2, METTL6, and METTL8. METTL2 can methylate tRNA$^{Thr}_{AGU}$, tRNA$^{Thr}_{UGU}$, and tRNA$^{Arg}_{CCU}$ (*22*). In line with this, we did not observe any effect of METTL6 KO on the methylation of these tRNA isoacceptors. METTL6 can interact with seryl-tRNA synthetases, and tRNA^{Ser} isoacceptors have been suggested as substrates (*22*). However, so far, direct biochemical evidence for catalytic activity of METTL6 was lacking. Our in vitro assays with recombinant METTL6 demonstrate that METTL6 is indeed a bona fide methyltransferase. Together with our cellular assays, this shows that METTL6 catalyzes the formation of m^{3}C at C32 in specific tRNAs^{Ser} isoacceptors, but not in other tRNAs that carry m^{3}C. Knockout of METTL6 only halves the m^{3}C levels in these tRNA^{Ser} isoacceptors, suggesting that the second m^{3}C site in the variable loop of these tRNA isoacceptors is methylated by another enzyme [e.g., METTL2 (*22*)]. Of note, we did not detect any major effects of METTL6 depletion on m^{3}C levels in the polyA-containing fractions in line with the suggestion of METTL8 being an mRNA methyltransferase (*22*).

We used *Mettl6* KO mES cells to study the effects of METTL6 loss on mRNA abundance and translation efficiency. We observed a widespread, correlated deregulation of both mRNA abundance and translation of mRNAs encoding genes related to proliferation, signaling, and growth control, as well as translation and proteostasis. These changes in the translational and transcriptional landscape could trigger cellular dysfunction directly (such as differentiation defects in the mESCs) and affect oncogenic programs (via cell cycle control or proliferation) or could be secondary biological changes resulting from, for example, growth defects.

Mettl6 KO mESCs display signs of impaired pluripotency as well as of compromised self-renewal potential. On the transcriptome level, we observed down-regulation of pluripotency and up-regulation of gastrulation and mesodermal markers. These impairments (but not total loss) of pluripotency and differentiation capacity are consistent with the fact that we were able to breed viable *Mettl6* KO mice. In both the mESC and HepG2 cells deficient in METTL6, we detected growth rate reductions. Albeit the underlying mechanisms might be different, this points toward an important function of METTL6 in both ESCs and transformed cells. This is in agreement with Gatza *et al.* (*37*), who also reported effects of METTL6 depletion on cell proliferation in human breast cancer cells, suggesting a role of METTL6 in cell growth in multiple, although not across all, cell types (*22*), pointing toward a cellular context–dependent function.

Our *Mettl6* KO mice develop normal phenotypes and did not show obvious morphological phenotypes; in line with this, Xu *et al.* (*22*) reported no evident phenotype. However, our systemic phenotyping of *Mettl6* KO mice revealed altered glucose homeostasis, changes in metabolic turnover, and decreased liver weight, suggesting a previously unknown impact of *Mettl6* on hepatic growth and on regulation of metabolism and energy balance at the whole-body level. This is supported by previous findings linking deregulation and/or mutation in tRNA-modifying enzymes to a variety of human diseases ranging from metabolic imbalances to different types of cancer (*34*, *38*). Of note, all the mouse studies were conducted in 16-week-old

mice (or younger) to exclude confounding effects of age; however, this did not allow us to observe spontaneous tumor formation.

Using a combination of in vitro and in vivo screens, we identified METTL6 as a potential new oncogene. In line with our findings that loss of METTL6 inhibits liver cancer cell proliferation and impaired colony formation capacity and capacity for anchorage-independent growth, low expression of METTL6 correlates with increased survival of patients with HCC. Given the recent success in identifying selective and potent small-molecule inhibitors of methyltransferases, RNA methyltransferases (*39*) such as METTL6 could thus represent novel therapeutic targets for antiproliferative cancer drugs. The role of METTL6 seems to extend beyond liver cancer as it has also been found amplified in different tumors such as highly proliferative luminal tumors (*32*). Here, once again, amplification of METTL6 predicts a significantly worse outcome for patients (*37*, *40*, *41*).

MATERIALS AND METHODS
shRNA screen
HepG2 cells were seeded 1 day before infection in 150-mm dishes. The next day, lentiviral pools were used to infect the cells at a multiplicity of infection (MOI) of 1 in the presence of polybrene (8 µg/ml). Lentiviral infected cells were then selected in puromycin (1 µg/ml) 48 hours after infection. The selection was deemed complete when 100% of cells in control uninfected plates were dead, which usually took place within 3 to 4 days after selection.

After selection, cells were harvested and used for either in vitro passaging or in vivo tumorigenesis studies. A fraction of these cells was also saved and used as the input (P0) control during sequencing. For in vitro passaging experiments, cells were harvested after every passage (~3 to 4 population doublings). Equal numbers of cells (1.5×10^6) were replated after each passage. Cell pellets were flash-frozen and stored at −80°C. For in vivo tumorigenesis studies, 3×10^6 cells were injected into the flanks of 6- to 8-week-old CB17-SCID mice (in vivo). Mice were then monitored for tumor growth every 2 to 3 days. Tumors formed around 3 weeks after injection. Tumors were harvested upon reaching sizes of 1000 mm^3. Tumors were dissociated into single cells in trypsin and pelleted via centrifugation. Cell pellets were then flash-frozen and stored at −80°C until further processing.

For library preparation, genomic DNA from either the in vitro or in vivo passaged tumor cells were harvested with the QIAGEN DNeasy kit following the manufacturer's protocol. As controls, RNA was also harvested from 3.5×10^6 infectious units of the virus using TRIzol. Lentiviral RNA was made into complementary DNA (cDNA) using the Invitrogen Maxima cDNA synthesis reagent. To synthesize the libraries, polymerase chain reaction (PCR) was performed on isolated genomic DNA using primers spanning the common 3′ and 5′ flanking sequences of the shRNA expression cassette. As input controls, the PCR was also performed on the starting plasmid pools and cDNA was prepared from RNA isolated from the pools of lentivirus. To enable high-throughput pooled sequencing, amplicon PCR primers included adaptors for Illumina sequencing. After PCR amplification, edgeR was used to map sequenced hairpins. Enrichment or depletion was determined by normalization to the starting pool of infected cells.

Reverse transcription quantitative PCR validation of METTL6 KD
HepG2 cells infected with either the scrambled or METTL6 targeting shRNAs (8G3, 8G5, and 8G6) were lysed in TRIzol. RNA from

TRIzol lysates was then isolated using the PureLink RNA Mini Kit (Thermo Fisher Scientific), including a deoxyribonuclease (DNase) (PureLink DNase Set, Thermo Fisher Scientific) treatment step. DNase-treated RNA (1 μg) was then reverse-transcribed into cDNA (Maxima First Strand cDNA synthesis kit; Thermo Fisher Scientific) using random hexamer primers and following the manufacturer's recommendations. cDNA (10 ng) was then used for each quantitative PCR, to quantify METTL6 and HPRT1 mRNA levels.

Human METTL6 F	AAAGACAGACACTGGACCACCA
Human METTL6 R	AACAGTTTCCAACCCCACAGC
Human HPRT1 F	TGCTGAGGATTTGGAAAGGG
Human HPRT1 R	ACAGAGGGCTACAATGTGATG

Cell culture

HAP1 wt and *METTL6* KO (obtained from Horizon Discovery clones: C631, HZGHC005030c008, HZGHC005031c011, and HZGHC005031c010) cells were cultured in high-glucose Iscove's modified Eagle's medium (IMEM) supplemented with 10% fetal bovine serum (FBS) and 1% penicillin-streptomycin (Life Technologies Inc.).

For CRISPR-assisted cell line generation, mESCs were maintained on 0.2% gelatin-coated dishes in DMEM (Sigma-Aldrich) supplemented with 16% FBS (Sigma), 0.1 mM β-mercaptoethanol (Invitrogen), 2 mM L-glutamine (Sigma-Aldrich), 1× minimum essential medium (MEM) nonessential amino acids (Sigma-Aldrich), penicillin (100 U/ml), streptomycin (100 μg/ml; Sigma-Aldrich), homemade recombinant LIF tested for efficient self-renewal maintenance, and 2i [1 μM PD032591 and 3 μM CHIR99021 (Axon Medchem, The Netherlands)]. All cell lines were regularly tested for mycoplasma contamination by PCR.

For Methyl-NAIL-MS of in vitro reactions, cells were cultured in the RPMI 1640 media (Sigma-Aldrich, product no. R7513) lacking methionine with the addition of L-methionine-methyl-D3 (98% atom) from Sigma-Aldrich, 10% FBS (Life Technologies Inc.), and 2 mM L-glutamine (Sigma-Aldrich) for 5 days. For comparative NAIL-MS of RNA from wt and *METTL6* KO, HAP1 cells were cultured in RPMI 1640 media (MP Biomedicals, Heidelberg, Germany, product no. 09 16468 5) lacking glucose with the addition of $^{13}C_6$-glucose (99% atom from Silantes, Munich, Germany) in case of KO cells and unlabeled glucose for wt cells, 0.01 mM adenine (Sigma-Aldrich), 10% dialyzed FBS (Sigma-Aldrich, product no. F0392-500ML), 0.06 mM methionine (Sigma-Aldrich), and 2 mM L-glutamine (Sigma-Aldrich) for 7 days.

CRISPR-Cas9 gene editing

For the generation of the *Mettl6* KO mutants, *Mettl6*-specific guide RNA s (gRNAs) were cloned into a modified version of the SpCas9-T2A-Puromycin/gRNA vector [px459 (*42*), Addgene plasmid #62988], where we fused truncated human Geminin to SpCas9 for increasing homology-directed repair efficiency. A pUC57 mini vector harboring a mNeonGreen PolyA cassette of 1068 and ~300 base pairs (bp) of homology to the genomic locus was synthesized (GenScript, Piscataway, NJ, USA). For targeting in wt J1 ESCs, cells were transfected with a 4:1 ratio of donor oligo and Cas9/gRNA construct. After 2 days of transfection, cells were subjected to a transient puromycin selection (1 μg/ml) for 48 hours and enriched by flow cytometry. Colonies were

allowed to grow for 6 days, at which point they were picked into 96-well plates, and screened using restriction fragment length polymorphism analysis. Cell lysis in 96-well plates, PCR on lysates, and restriction digest were performed as previously described (*43*). For all cell lines, *Mettl6* mutation was confirmed by Sanger sequencing.

The following oligonucleotides were used:

Mettl6 gRNA FWD	CACCGCTACAATGGCTTCTTTCCAA
Mettl6 gRNA REV	aaacTTGGAAAGAAGCCATTGTAGC
Mettl6_scr_FWD	GCAGGCAGGTTGTTAGAGAATCACT
Mettl6_scr_REV	CAAATCAGAACTCTCCATAGGTACA
Mettl6_InsertScr_FWD	tgatgggcatggacgagctg
Mettl6_InsertScr_REV	aagtccacaccgttgatggagc
mNeonGreen-Poly donor with homology arms	CCTAAGTAGCATCGTATCCTGTTGGAGCTGGAAAGTCACCTGGGGAAACTGCATCAGAGAAACTCCAGTGTCTACAATCTCAGCATCGTTTGTTCAGATGGTTGAAGAACAGAGGACCTATAGCAGCATTGAATGTGTTTCCGGCAACTACAATGGCTTCTTTCgtgagcaagggcgaggaggataacatggcctctctccagcgacacatgagttacacatctttggctccatcaacggtgtggactttgacatggtgggtcagggcaccggcaatccaaatgatggttatgaggagttaaactgaagtccaccaagggtgactccagttctcccctggattctggtccctcatatcgggtatggcttccatcagtacctgccctaccctgacgggatgtcgcctttccaggccgccatggtagatggctccggataccaagtccatcgcacaatgcagtttgaagatggtgcctcccttactgttaactaccgctacacctacgagggaagccacatcaaaggagaggcccaggtgaagggggactggtttccctgctgacggtcctgtgatgaccaactcgctgaccgctgcggactggtgcaggtcgaagaagacttaccccaacgacaaaaccatcatcagtacctttaagtggagttacaccactggaaatggcaagcgctaccggagcactgcgcggaccacctacaccttgccaagccaatggcggctaactatctgaagaaccagccgatgtacgtgttccgtaagacggagctcaagcactccaagaccgagctcaacttcaaggagtggcaaaaggcctttaccgatgtgatgggcatggacgagctgtgtacaagtaagatccagacatgataagatacattgatgagtttggacaaaccacaactagaatgcagtgaaaaaaatgcttttatttgtgaaatttgtgatgctattgctttatttgtaaccattataagctgcaataaacaagttaacaacaacaattgcattcattttatgtttcaggttcaggggggaggtgtgggaggttttttCAAAGGAAAGGACTGCAAGCAAGGATTCTTAGCACTGAAGAAGAGGAGAAACTGAAAAGAGACCAAGCTTTGGTGTCTGCTTTTAAACAGCAAAAACTGGAAAAAGAGGCTCAGAAGAACTGGGACCTTTTTTATAAAAGAAACAGTACCAATTTTTTCAAGGACAGACACTGGACCACCAGAGAGTTTGAGGAGTTGAGATCATGTAGGGAGGTAGGCTGGGGTTTCTCCTGGCTCGAGCCATCTTCATTTATGATGCCTAGAAGAGAGGTCCTTTGTTACATGTAGAGAGTGCTC

AP staining

For AP staining, 5000 cells (wt and *Mettl6* KO clones #D1 and #G6) were seeded, and after 5 days, cells were fixed (4% formaldehyde) and stained for AP with Alkaline Phosphatase Blue Membrane Substrate Solution (Sigma-Aldrich, AB0300), according to the manufacturer's protocol. mESCs were cultured on 0.2% gelatin-coated dishes in DMEM

(Sigma-Aldrich) supplemented with 16% FBS (Sigma-Aldrich), 0.1 mM β-mercaptoethanol (Invitrogen), 2 mM L-glutamine (Sigma-Aldrich), 1× MEM nonessential amino acids (Sigma-Aldrich), penicillin (100 U/ml), streptomycin (100 μg/ml; Sigma-Aldrich), and homemade recombinant LIF tested for efficient self-renewal maintenance.

EB formation

For EB formation, mESCs (wt and *Mettl6* KO clones #D1 and #G6) were cultured for 8 days in serum-LIF media. A total of 4×10^6 mESCs were seeded on bacteriological petri dishes cultured in DMEM (Sigma-Aldrich) supplemented with 10% FBS (Sigma-Aldrich), 0.1 mM β-mercaptoethanol (Invitrogen), 2 mM L-glutamine (Sigma-Aldrich), 1× MEM nonessential amino acids (Sigma-Aldrich), penicillin (100 U/ml), and streptomycin (100 μg/ml; Sigma-Aldrich). Every second day, EBs were transferred to a new petri dish.

Immunoblots

mESC extracts were prepared by lysis of the cell pellets in the five volumes of the lysis buffer [50 mM tris (pH 8), 150 mM NaCl, 0.5 mM dithiothreitol (DTT), 0.5% NP-40, 10% glycerol, and protease inhibitors] for 30 min at 4°C with rotation. Lysates were centrifuged for 30 min at 4°C at maximum speed, and supernatants were collected. Total protein concentration was measured with the Pierce BCA Protein Assay Kit (Thermo Fisher Scientific). A whole-cell extract (20 μg) was loaded per lane on 10% tris-glycine gels, ran in SDS–polyacrylamide gel electrophoresis (SDS-PAGE) buffer using the Bio-Rad Mini-PROTEAN system at 125 V, and transferred to a nitrocellulose membrane, followed by blocking and immunostaining. The antibodies used were as follows: anti-METTL6 (1:5000 dilution; HPA035166, Sigma-Aldrich) primary antibody followed by horseradish peroxidase–conjugated secondary antibodies anti-rabbit (1:100,000, 111-035-003, the Jackson Laboratory). HepG2 cells were lysed in 1× Laemmli buffer and sonicated for 10 s using the Qsonica Q55 sonicator. After PAGE and transfer, membranes were blocked before they were incubated overnight at 4°C with either the METTL6 (1:1000 dilution; HPA035166, Sigma-Aldrich) or glyceraldehyde phosphate dehydrogenase (1:1000 dilution; Santa Cruz Biotechnology, sc-32233) antibodies. This was followed by three 5-min washes in phosphate-buffered saline (PBS) + 0.1% Tween and incubation with secondary antibody and exposure using Supersignal West Pico Chemiluminescent substrate (Thermo Fisher Scientific).

Generation of METTL6 mutants

A plasmid encoding GST-METTL6 was obtained from OriGene (catalog no. EX-H0241-B06, accession no. NM_152396). GST-METTL6 N92A and F111A mutants were cloned by Q5 site-directed mutagenesis following the standard protocol from New England Biolabs and verified by Sanger sequencing. Mutagenesis primers were as follows:

Oligo	Sequence (5′-3′)
METTL6_N92A_F	TGGGGTTGGAgcCTGTTTATTCCCAC
METTL6_N92A_R	CAGCCAGCTTCAAGCATT
METTL6_F111A_F	TGCCTGTGATgcTTCTCCAAGAG
METTL6_F111A_R	TAGGCAAAGATATTCGGATC

GST, GST-METTL6, GST-METTL6 N92A, and F111A protein purification

BL21 Golds (DE3) *Escherichia coli* were transformed with plasmids for recombinant protein expression followed by induction with 0.5 M isopropyl-β-D-thiogalactopyranoside at 18°C overnight. *E. coli* were harvested, and cell pellets were lysed in 25 mM tris-HCl (pH 8), 150 mM NaCl, 1 mM EDTA, 0.5% Triton X-100, and 0.2 mM phenylmethylsulfonyl fluoride (PMSF) with mild sonication. Lysates were centrifuged at 20,000g for 30 min at +4°C, and supernatants were collected and incubated with glutathione Sepharose beads (GE Healthcare) for 4 hours at 4°C with rotation, followed by washes with lysis buffer (with NaCl adjusted to 300 mM), competitive elution with 10 mM reduced glutathione in 50 mM tris-HCl (pH 8.0), and dialysis overnight against buffer for gel filtration chromatography [15 mM Hepes (pH 8.0), 1 mM EDTA, 1 mM DTT, 0.2 mM PMSF, and 4% glycerol]. Gel filtration chromatography was performed with a Superdex 200 Increase 10/300 GL column using an ÄKTA pure system (column volume, 23.562 ml; flow rate, 0.75 ml/min; software, UNICORN 6.4) according to a standard protocol. Samples were eluted with 1.5 column volumes, and 450-μl fractions were collected for PAGE and in vitro methyltransferase assays. The equilibration and elution buffer consists of 15 mM Hepes (pH 8.0), 1 mM EDTA, 1 mM DTT, 0.2 mM PMSF, and 4% glycerol.

In vitro methyltransferase assay

Methyltransferase assays were performed in 6 mM Hepes-KOH (pH 8), 0.4 mM EDTA, 10 mM DTT, 80 mM KCl, 1.5 mM MgCl$_2$, RNasin (0.2 U/ml), and 1.6% glycerol, in the presence of 460 nM [3H]-SAM (PerkinElmer). Five micrograms of total RNA prepared from HeLa cells or 200 ng of in vitro transcribed tRNA per reaction was used as a substrate. Assays were performed at +16°C overnight, followed by acid phenol chloroform extraction and column purification with the Zymo Research RNA miniprep kit. Tritium incorporation was analyzed by liquid scintillation counting using a Triathler counter (Hidex) in Ultima Gold liquid scintillation counting cocktail (PerkinElmer) and shown as counts per minute. All data of in vitro methyltransferase assays are shown as means ± SD from three replicates. For nonradioactive assays, 80 μM SAM (New England Biolabs, B9003S) was used as methyl group donor per reaction.

Size exclusion chromatography

For purification of total RNA or purification of tRNA (either native or in vitro transcripts from precursor products), size exclusion chromatography was used on an Agilent 1100 high-performance LC (HPLC) system (Degasser, G1279A; Quad Pump, G1311A; ALS, G1313A; COLCOM, G1316A; VWD, G1314A; Analyt FC, G1364C) using an AdvanceBio 300 Å or 130 Å (Agilent, Waldbronn, Germany; part no. 1180-5301). The column temperature was set to 40°C for native tRNA purification using the AdvanceBio 300 Å and to 60°C for in vitro transcript purification using the AdvanceBio 130 Å. For elution, an isocratic flow (1 ml/min) of 0.1 M ammonium acetate was used. Eluting RNA was detected at 254 nm with a diode array detector. The eluted RNA was collected by a fraction collector, and the eluent was evaporated (GeneVac, EZ-2 PLUS, Ipswich, UK) to a volume of ~50 μl before ethanol precipitation. The purified RNA was dissolved in 30 μl of water for further enzymatic assays or MS analysis.

Gel purification of RNA

RNA of the size range of 20 to 200 nt was purified from total RNA using the Zymo Research RNA miniprep kit by standard protocol.

RNA (20 μg) was loaded per well of a 12% urea gel (prepared according to the standard protocol from National Diagnostics), RNA fragments in the size range of 70 to 80 nt and ~85 nt were excised from the gel, and the gel was homogenized and snap-frozen in liquid nitrogen in the presence of three volumes of 1× TBE (tris-borate EDTA buffer) buffer. RNA was recovered by four subsequent cycles of thawing and snap freezing in liquid nitrogen, followed by isopropanol precipitation at −80°C overnight.

For rescue experiment (fig. S3C), RNA was isolated from mESC wt and *Mettl6* KO clone #D1 transiently transfected with either GFP-METTL6 or GFP-METTL6 N92A using Xfect mESC Transfection Reagent (Takara Bio) followed by fluorescence-activated cell sorting (FACS) to enrich green fluorescent protein (GFP)–positive cells and the second round of transfection.

tRNA isoacceptor isolation
tRNA isoacceptors were isolated as previously reported (*44*). The DNA probes listed in table S2 were purchased from Sigma-Aldrich.

Enzymatic digestion of RNA for MS
Three-microgram to 100-ng portions of RNA were digested to single nucleosides with AP (0.2 U; Sigma-Aldrich, St. Louis, MO, USA), phosphodiesterase I (0.02 U; VWR, Radnor, PA, USA), and Benzonase (0.2 U) in tris (pH 8, 5 mM)– and $MgCl_2$ (1 mM)–containing buffer. Furthermore, tetrahydrouridine (0.5 μg from Merck), butylated hydroxytoluene (1 μM), and pentostatin (0.1 μg) were added to protect modification (*45*). The mixture was incubated with the RNA for 2 hours at 37°C. Afterward, samples were filtered through 96-well filter plates (AcroPrep Advance 350 10K Omega, Pall Corporation, NY, USA) for longer than 10 min at 3000*g* to remove digestive enzymes.

LC-MS/MS analysis of in vitro methylated RNA
Ribonucleosides were separated using a Luna Omega Polar (150 × 2.1 mm; particle size, 2.5 μm; pore size, 100 Å; Phenomenex, Torrance, CA) on an Agilent 1290 series HPLC system equipped with a diode array detector. Mobile phase A was 5 mM NH_4OAc (≥99%; HiPerSolv CHROMANORM, VWR) adjusted to pH 5.3 with glacial acetic acid (≥99%, HiPerSolv CHROMANORM, VWR), and mobile phase B was pure acetonitrile (LC-MS grade, purity ≥99.95; Roth). Gradient elution started with 98% A and increased to 10% B after 2 min, 30% B after 3 min, and 60% B after 3.5 min. Starting conditions are re-established at 4 min followed by 2 min of equilibration. The flow rate was 0.4 ml/min, and the column temperature was 30°C. The effluent from the column was directed through the DAD (diode array detector) before entering the Agilent 6490 Triple Quadrupole mass spectrometer in dynamic multiple reaction monitoring (MRM) mode. The MS was operated in positive-ion mode with the following parameters: electrospray ionization (ESI-MS, Agilent Jetstream); fragmentor voltage, (set in tunefile to) 250 V; cell accelerator voltage, 2 V; N_2-gas temperature, 150°C; N_2-gas flow, 15 liters/min; nebulizer, 30 psi; sheath gas (N_2) temperature, 275°C; sheath gas flow, 11 liters/min; capillary, 2500 V; and nozzle voltage, 500 V. The instrument was operated in dynamic MRM mode with the method listed in table S2.

LC-MS/MS analysis of in vivo methylated RNA
For quantification, an Agilent 1290 Infinity II equipped with a DAD combined with an Agilent Technologies G6470A Triple Quad system and electrospray ionization (ESI-MS, Agilent Jetstream) was used.

Operating parameters were as follows: positive-ion mode; skimmer voltage, 15 V; cell accelerator voltage, 5 V; N_2 gas temperature, 230°C; N_2 gas flow, 6 liters/min; sheath gas (N_2) temperature, 400°C with a flow of 12 liters/min; capillary voltage, 2500 V; nozzle voltage, 0 V; and nebulizer, 40 psi. The instrument was operated in dynamic MRM mode with the method listed in table S2. The mobile phases were as follows: A as 5 mM NH_4OAc aqueous buffer, brought to pH 5.6 with glacial acetic acid, and B as pure acetonitrile. A Synergi Fusion-RP column (Phenomenex, Torrance, CA, USA; Synergi 2.5 μm Fusion-RP 100 Å, 150 × 2.0 mm) at 35°C and a flow rate of 0.35 ml/min was used. The gradient began with 100% A for 1 min and increased to 10% B by 5 min and to 40% B by 7 min. The column was flushed with 40% B for 1 min and returned to starting conditions to 100% A by 8.5 min followed by re-equilibration at 100% A for an additional 2.5 min. For quantification, a stable isotope-labeled internal standard (*46*) was added to the samples before injection. Data analysis was performed as previously described (*46*).

In vitro transcription of tRNA
tRNA$^{Ser}_{UGA}$ was transcribed by ribozyme fusion transcription as reported by Fechter *et al.* (*28*). All PCRs were performed in a total volume of 50 μl with a final concentration of onefold Phusion HF Buffer (New England Biolabs, Ipswich, MA) and 0.8 μM forward and reverse primers. The sequence of templates and primers is given below. In addition, 1 μl of deoxynucleotide triphosphates, 0.5 μl of Phusion polymerase, and 100 ng of the desired DNA template were added. All samples were amplified with the same PCR program: 95°C for 2 min and 95°C for 30 s. For 20 amplification cycles, 57°C for 30 s 20 times and 68°C for 1 min 20 times. At the end of the program, the PCR was incubated at 68°C for 1 min and was cooled down to 4°C. Every PCR was performed twice and pooled afterward for the T7 in vitro transcription. Primers and templates used for T7 in vitro transcription were as follows:

T7 transcription/PCR forward primer	TGGCGTAGTCGGC
T7 transcription/PCR reverse primer	CGCGCGAAGCTTAATACGACTCACTATA
T7 transcription/PCR template wt	TGG CGT AGT CGG CAG GAT TCG AAC CTG CGC GGG GAA ACC CCA ATG GAT TTC AAG TCC ATC GCC TTA ACC ACT CGG CCA CGA CTA CGA CGG TAC CGG GTA CCG TTT CGT CCT CAC GGA CTC ATC AGG TAG TCG TGT CTC CCT ATA GTG AGT CGT ATT
T7 transcription/PCR template wt U47dC	TGG CGT AGT CGG CAG GAT TCG AAC CTG CGC GGG GAG ACC CCA ATG GAT TTC AAG TCC ATC GCC TTA ACC ACT CGG CCA CGA CTA CGA CGG TAC CGG GTA CCG TTT CGT CCT CAC GGA CTC ATC AGG TAG TCG TGT CTC CCT ATA GTG AGT CGT ATT
T7 transcription/PCR template wt C32G	TGG CGT AGT CGG CAG GAT TCG AAC CTG CGC GGG GAG ACC CCA ATG GAT TTC AAC TCC ATC GCC TTA ACC ACT CGG CCA CGA CTA CGA CGG TAC CGG GTA CCG TTT CGT CCT CAC GGA CTC ATC AGG TAG TCG TGT CTC CCT ATA GTG AGT CGT ATT

The total volume of the T7 in vitro transcription was 200 μl. PCR product (100 μl) was added to a T7 buffer mix and T7 enzyme (TranscriptAid T7 High Yield Transcription Kit, Thermo Fisher

Scientific, Waltham, MA) and 1.6 μl of each rNTP (Ribonucleotide Triphosphates). The mixture was incubated for 2 hours at 37°C and 600 rpm. After 2-hour incubation, the sample was treated with 2 μl of T7 enzyme mix and 5 μl of 50 mM $MgCl_2$ and incubated for an additional 2 hours. After another 2-hour incubation, the sample was treated again with 2 μl of T7 enzyme mix and 5 μl of 50 mM $MgCl_2$ and incubated for an additional 2 hours to improve the yield of the transcription. DNA template was removed by the addition of 4 μl of DNase I, which is provided in the kit, 1 hour for 37°C. In the next step, $MgCl_2$ was added with a final concentration of 5 mM, and the sample was incubated at 60°C for 1 hour to autocatalytically cleave the precursor in vitro transcript into its target tRNA. Before RNA precipitation, the sample was centrifuged at 5000g for 5 min at room temperature to remove the insoluble pyrophosphate of the transcription reaction. The supernatant was precipitated by the addition of 0.1 volumes of 5 M ammonium acetate and 2.5 volumes of ice-cold ethanol (100%) followed by overnight incubation at −20°C. The RNA was pelleted by centrifugation (12,000g, 40 min, 4°C), washed with 70% ethanol, and resuspended in 30 μl of water.

Cell growth measurements
HepG2 cells [stably expressing the scramble, 8G3 (TRCN0000151394), 8G4 (TRCN0000157967), and 8G5 (TRCN0000150694) shRNAs] were seeded 1 day before infection in 150-mm dishes. The next day, lentiviruses expressing hairpins of interest were then used to infect the cells at an MOI of 1 in the presence of polybrene (8 μg/ml). Lentiviral infected cells were then selected in puromycin (1 μg/ml) for 48 hours after infection. The selection was deemed complete when 100% of cells in control uninfected plates were dead; this usually took place within 3 to 4 days after selection. Upon completion of selection, cells were trypsinized and counted. A total of 2×10^5 cells were plated into a six-well plate and allowed to attach. Cell growth was determined by trypsinizing and counting cells at the indicated time points.

Wt and *Mettl6* KO mESC (clones #D1, #G6, and #F8) were seeded 2 days before measurements at a density of 500 cells per well in 96-well plates. At each time point, cells were lysed on ice in 10 mM tris (pH 8), 1 mM EDTA, and 0.2% Triton X-100. Cell numbers were determined using the Quant-iT PicoGreen dsDNA Assay Kit (Invitrogen) and standard curve following the manufacturer's protocol.

Colony formation assays
For colony formation assays, HepG2 cells stably expressing scramble, 8G3 (TRCN0000151394), 8G4 (TRCN0000157967), and 8G5 (TRCN0000150694) shRNAs were plated at a density of 1×10^4 cells per six-well plate and allowed to proliferate for 7 days. Colonies were then fixed in 5% formaldehyde in PBS and stained using 1% crystal violet solution. Plates were scanned and colony areas were determined using the ImageJ ColonyArea plugin.

Soft agar assay
One milliliter of culture medium (DMEM + 10% FBS + penicillin/streptomycin) with 0.3% agar (Oxoid) was first plated into each well of a six-well plate. After the agar was solidified, 7500 cells were resuspended in 2 ml of 0.3% agar in culture medium and were plated into each well. One milliliter of culture medium (DMEM + 10% FBS + penicillin/streptomycin) was overlaid. After 1 week in culture, agar plugs were fixed in 1% formaldehyde and stained with 0.1% crystal violet. After destaining in water, agar plugs were photographed, and colonies were manually counted.

Cell cycle analysis in HepG2 cells
Exponentially growing HepG2 cells were trypsinized and washed twice in PBS. Samples were then fixed in 70% ethanol overnight at −20°C. Fixed samples were then pelleted and washed twice in wash buffer (PBS + 10% FBS + 0.1% Triton X-100). All centrifugation steps were performed at 2000 rpm for 5 min at 4°C. The pellet was then resuspended in staining buffer [PBS + 10% FBS + 0.1% Triton X-100 + ribonuclease A (Rnase A, 50 μg/ml) (Thermo Fisher Scientific, EN0531) + Hoechst 33342 (20 μg/ml; BD Biosciences; 561908)]. Cells were stained at room temperature in the dark for 1 hour before they were passed on a 20-μm membrane and analyzed on the BD FACSCanto II. Cell cycle analysis was performed using FCS Express 7 software.

Flow cytometric analysis of mESCs
For apoptosis and cell cycle assay, mESCs (wt and *Mettl6* KO clones #D1 and #G6) grown in serum-LIF for 6 days were stained with annexin V/propidium iodide according to the manufacturer's protocol (Annexin V Apoptosis Detection Kit FITC, eBioscience) or fixed in ethanol and stained with propidium iodide correspondingly followed by flow cytometry analysis. Events were recorded by the FACSAria III Sorter and analyzed with the FlowJo 10.6.1 software. Sequential electronic gating was performed to obtain single cells. Cell cycle analysis was performed in FlowJo 10.6.1.

Ribosome profiling and RNA-seq
Ribosome profiling was carried out based on the study of Ingolia *et al.* (*47*) with minor modifications using wt and *Mettl6* KO clone #G6 mESCs grown in serum-LIF supplemented with 2i. Briefly, translation was blocked by cycloheximide (100 μg/ml) for 10 min and washed on ice, and cytoplasmic extract was prepared by repeated pipette homogenization using freshly prepared ice-cold lysis buffer [10 mM tris-HCl (pH 7.5), 5 mM $MgCl_2$, 100 mM KCl, 1% Triton X-100, 2 mM DTT, cycloheximide (100 μg/ml), and EDTA-free complete protease inhibitor] and snap-frozen. For ribosome footprinting, we used RNase A + T1 instead of RNase I, which has been found to be detrimental to mammalian ribosome integrity (*48*). Cell lysates were incubated with 60 U of RNase T1 and 30 U of RNase A per A_{260} absorbance unit of cell extract at room temperature and then loaded onto a 10 to 50% (w/v) sucrose gradient [20 mM Hepes-KOH (pH 7.4), 5 mM $MgCl_2$, 100 mM KCl, 2 mM DTT, and cycloheximide (100 μg/ml)] and spun at 35K rpm for 2 hours and 40 min in a SW40Ti rotor. The 80S fraction was collected, and total RNA was collected using an equal volume of TRIzol followed by isopropanol precipitation. RNAs (26 to 32 nt in size) were isolated from total RNA by running the samples on a 15% denaturing acrylamide gel.

During cell extract preparation, a small fraction of the sample was left aside, and total RNA was extracted using TRIzol followed by isopropanol precipitation. Ribosomal RNA was removed using the Ribo-Zero rRNA Removal Kit (Illumina) and fragmented using RNA Fragmentation Reagent (Ambion). Fragmented RNA and ribosome footprint RNA were cloned using a circularization method described by Heyer *et al.* (*49*). Final libraries were pooled and single-end sequenced on a NextSeq 500 (Illumina).

RNA-seq and data analysis
Library preparation was performed using the TruSeq Stranded Total RNA Library Prep Kit with Ribo-Zero (Illumina). Briefly, RNA from wt and Mettl6 KO clone #D1 and #G6 mESCs grown under serum-LIF

conditions was isolated using the NucleoSpin RNA miniprep kit (Macherey-Nagel), and RNA integrity number was determined with the Agilent 2100 BioAnalyzer (RNA 6000 Nano Kit, Agilent). For library preparation, 1 μg of total RNA was depleted for cytoplasmic ribosomal RNAs (rRNAs), fragmented, and reverse-transcribed with the Elute, Prime, Fragment Mix. A-tailing, adaptor ligation, and library enrichment were performed as described in the High Throughput protocol of the TruSeq stranded total RNA Sample Prep Guide (Illumina). RNA libraries were assessed for quality and quantity with the Agilent 2100 BioAnalyzer and the Quant-iT PicoGreen dsDNA Assay Kit (Life Technologies).

RNA libraries were sequenced as 150-bp paired-end runs on an Illumina HiSeq 4000 platform. Sequencing was performed at the Helmholtz Zentrum München (HMGU) by the NGS-Core Facility. RNA-seq libraries were processed and mapped to the mouse genome (mm10) using STAR v2.5.3a (50) with a quantMode GeneCounts option. Count tables were filtered for low counts using HTSFilter v1.18.0 (51). Differential expression analysis was performed in R using DESeq2 v1.18.1 (52), and genes with an adjusted $P < 0.05$ and an log2 FC" (fold change) > |1| were considered to be differentially expressed. GO analysis was performed using the topGO v2.30.1 in combination with org.Mm.eg.db v3.5.0. KEGG (Kyoto Encyclopedia of Genes and Genomes) pathway analysis was performed using the KEGGprofile v1.20.0 package.

Genotype analysis
Genomic DNA was extracted from tissue samples collected from mice during ear labeling at weaning age (3 weeks old), and PCR was performed with the following *Mettl6*-specific primers: *Mettl6*-F: tgtactccacacctgacatgg and *Mettl5*-R: cctgttggcatcacatgacag.

Intraperitoneal GTT
Mice were used for the GTT after a 16- to 18-hour–lasting food withdrawal. Before food withdrawal and in the beginning of the test, the body weight of mice was determined. For the determination of the fasting blood glucose level, the tip of the tail was scored using a sterilized scalpel blade, and a small drop of blood was analyzed with the Accu-Chek Aviva glucose analyzer (Roche/Mannheim). Thereafter, mice were injected intraperitoneally with 2 g of glucose per kilogram of body weight using a 20% glucose solution, a 25-gauge needle, and a 1-ml syringe. Fifteen, 30, 60, and 120 min after glucose injection, additional blood samples (one drop each) were collected and used to determine blood glucose levels as described before. Repeated bleeding was induced by removing the clot from the first incision and massaging the tail of the mouse. After the experiment was finished, mice were placed in a cage with plentiful supply of water and food.

Energy expenditure
Gas exchange (oxygen consumption and carbon dioxide production) of single-caged mice was measured by indirect calorimetry. Energy expenditure and respiratory quotient were calculated, as well as distance traveled and food and water intake. A cohort, composed of 10 female and 13 male controls and 10 male and 10 female mutants, was tested at 11 weeks of age as previously described (53).

Clinical chemistry
The analyses were performed using a Beckman Coulter AU 480 autoanalyzer and adapted reagents from Beckman Coulter (Krefeld, Germany),

except free fatty acids (NEFA) that were measured using a kit from Wako Chemicals GmbH (NEFA-HR2, Wako Chemicals, Neuss, Germany) and glycerol, which was measured using a kit from Randox Laboratories GmbH (Krefeld, Germany). In the primary screen, a broad set of parameters was measured including various enzyme activities, as well as plasma concentrations of specific substrates and electrolytes in ad libitum fed mice (54). A set of six measured parameters and one calculated value (blood lipid and glucose levels) is determined in samples derived from mice after overnight food withdrawal, if requested.

Liver sectioning and staining
For histopathological analyses, hematoxylin and eosin staining was performed on formalin-fixed paraffin-embedded sections (3 μm) of median lobe of the liver. The slides were analyzed by two independent pathologists.

Mouse line
Mettl6$^{-/-}$ mice (C57BL/6NJ-*Mettl6*$^{em1(IMPC)J}$/Mmjax, stock #31590) were obtained from the Jackson Laboratory (Bar Harbor, MN). Mice were maintained in IVC (individually ventilated cages) cages with water and standard mouse chow according to the directive 2010/63/EU, German laws, and GMC (German Mouse Clinic) housing conditions.

Ribosome sequencing data analysis
Single-end libraries were demultiplexed using in-line barcodes with NovoBarcode (Novocraft V3.02.08), and adapters were removed, keeping only reads >26 nt using the Fastx toolkit (V0.0.14). Reads were mapped with Bowtie (v1.0.0) to mm10 using default parameters. RPKM (Reads Per Kilobase Million)/TPM (transcripts per million) per gene (National Center for Biotechnology Information Refseq) for both ribosome footprint density and RNA abundance was counted by RSEM (V1.3). Differential expression was calculated using DESeq2 in R (V3.6). Translational efficiency was calculated by taking the $\log_2$ delta of the relative TPM of ribosome footprint density by relative TPM of RNA abundance, per biological replicate. For Fig. 5A, the $\log_2$ FC of TPMs for each replicate (wt or Mettl6 KO) to the average of the two wt replicates was calculated for each individual transcript for ribosome sequencing and for the corresponding total RNA-seq.

REFERENCES AND NOTES
1. K. Sarma, D. Reinberg, Histone variants meet their match. *Nat. Rev. Mol. Cell Biol.* **6**, 139–149 (2005).
2. A. J. Bannister, T. Kouzarides, Regulation of chromatin by histone modifications. *Cell Res.* **21**, 381–395 (2011).
3. T. Pan, Modifications and functional genomics of human transfer RNA. *Cell Res.* **28**, 395–404 (2018).
4. H. Ma, X. Wang, J. Cai, Q. Dai, S. K. Natchiar, R. Lv, K. Chen, Z. Lu, H. Chen, Y. G. Shi, F. Lan, J. Fan, B. P. Klaholz, T. Pan, Y. Shi, C. He, N6-Methyladenosine methyltransferase ZCCHC4 mediates ribosomal RNA methylation. *Nat. Chem. Biol.* **15**, 88–94 (2019).
5. P. Boccaletto, M. A. Machnicka, E. Purta, P. Piatkowski, B. Baginski, T. K. Wirecki, V. de Crécy-Lagard, R. Ross, P. A. Limbach, A. Kotter, M. Helm, J. M. Bujnicki, MODOMICS: A database of RNA modification pathways. 2017 update. *Nucleic Acids Res.* **46**, D303–D307 (2018).
6. H. Shi, J. Wei, C. He, Where, when, and how: Context-dependent functions of RNA methylation writers, readers, and erasers. *Mol. Cell* **74**, 640–650 (2019).

7. X. Deng, R. Su, H. Weng, H. Huang, Z. Li, J. Chen, RNA N6-methyladenosine modification in cancers: Current status and perspectives. *Cell Res.* **28**, 507–517 (2018).

8. S. Blanco, R. Bandiera, M. Popis, S. Hussain, P. Lombard, J. Aleksic, A. Sajini, H. Tanna, R. Cortés-Garrido, N. Gkatza, S. Dietmann, M. Frye, Stem cell function and stress response are controlled by protein synthesis. *Nature* **534**, 335–340 (2016).

9. N. Guzzi, M. Cieśla, P. C. T. Ngoc, S. Lang, S. Arora, M. Dimitriou, K. Pimková, M. N. E. Sommarin, R. Munita, M. Lubas, Y. Lim, K. Okuyama, S. Soneji, G. Karlsson, J. Hansson, G. Jönsson, A. H. Lund, M. Sigvardsson, E. Hellström-Lindberg, A. C. Hsieh, C. Bellodi, Pseudouridylation of tRNA-derived fragments steers translational control in stem cells. *Cell* **173**, 1204–1216.e26 (2018).

10. S. Lin, Q. Liu, V. S. Lelyveld, J. Choe, J. W. Szostak, R. I. Gregory, Mettl1/Wdr4-mediated m7G tRNA methylome is required for normal mRNA translation and embryonic stem cell self-renewal and differentiation. *Mol. Cell* **71**, 244–255.e5 (2018).

11. V. V. Ignatova, P. W. T. C. Jansen, M. P. Baltissen, M. Vermeulen, R. Schneider, The interactome of a family of potential methyltransferases in HeLa cells. *Sci. Rep.* **9**, 6584 (2019).

12. Q. H. Tian, M. F. Zhang, J. S. Zeng, R. G. Luo, Y. Wen, J. Chen, L. G. Gan, J. P. Xiong, METTL1 overexpression is correlated with poor prognosis and promotes hepatocellular carcinoma via PTEN. *J. Mol. Med.* **97**, 1535–1545 (2019).

13. C. R. Alarcón, H. Lee, H. Goodarzi, N. Halberg, S. F. Tavazoie, N⁶-methyladenosine marks primary microRNAs for processing. *Nature* **519**, 482–485 (2015).

14. I. Barbieri, K. Tzelepis, L. Pandolfini, J. Shi, G. Millán-Zambrano, S. C. Robson, D. Aspris, V. Migliori, A. J. Bannister, N. Han, E. De Braekeleer, H. Ponstingl, A. Hendrick, C. R. Vakoc, G. S. Vassiliou, T. Kouzarides, Promoter-bound METTL3 maintains myeloid leukaemia by m6A-dependent translation control. *Nature* **552**, 126–131 (2017).

15. L. Pandolfini, I. Barbieri, A. J. Bannister, A. Hendrick, B. Andrews, N. Webster, P. Murat, P. Mach, R. Brandi, S. C. Robson, V. Migliori, A. Alendar, M. d'Onofrio, S. Balasubramanian, T. Kouzarides, METTL1 promotes let-7 microRNA processing via m7G methylation. *Mol. Cell* **74**, 1278–1290.e9 (2019).

16. M. O'Connell, RNA modification and the epitranscriptome; the next frontier. *RNA* **21**, 703–704 (2015).

17. S. Delaunay, M. Frye, RNA modifications regulating cell fate in cancer. *Nat. Cell Biol.* **21**, 552–559 (2019).

18. F. Rapino, S. Delaunay, F. Rambow, Z. Zhou, L. Tharun, P. De Tullio, O. Sin, K. Shostak, S. Schmitz, J. Piepers, B. Ghesquière, L. Karim, B. Charloteaux, D. Jamart, A. Florin, C. Lambert, A. Rorive, G. Jerusalem, E. Leucci, M. Dewaele, M. Vooijs, S. A. Leidel, M. Georges, M. Voz, B. Peers, R. Büttner, J. C. Marine, A. Chariot, P. Close, Codon-specific translation reprogramming promotes resistance to targeted therapy. *Nature* **558**, 605–609 (2018).

19. R. Esteve-Puig, A. Bueno-Costa, M. Esteller, Writers, readers and erasers of RNA modifications in cancer. *Cancer Lett.* **474**, 127–137 (2020).

20. J. G. Tate, S. Bamford, H. C. Jubb, Z. Sondka, D. M. Beare, N. Bindal, H. Boutselakis, C. G. Cole, C. Creatore, E. Dawson, P. Fish, B. Harsha, C. Hathaway, S. C. Jupe, C. Y. Kok, K. Noble, L. Ponting, C. C. Ramshaw, C. E. Rye, H. E. Speedy, R. Stefancsik, S. L. Thompson, S. Wang, S. Ward, P. J. Campbell, S. A. Forbes, COSMIC: The catalogue of somatic mutations in cancer. *Nucleic Acids Res.* **47**, D941–D947 (2019).

21. D. Wu, E. Lim, F. Vaillant, M.-L. Asselin-Labat, J. E. Visvader, G. K. Smyth, ROAST: Rotation gene set tests for complex microarray experiments. *Bioinformatics* **26**, 2176–2182 (2010).

22. L. Xu, X. Liu, N. Sheng, K. S. Oo, J. Liang, Y. H. Chionh, J. Xu, F. Ye, Y. G. Gao, P. C. Dedon, X. Y. Fu, Three distinct 3-methylcytidine (m3C) methyltransferases modify tRNA and mRNA in mice and humans. *J. Biol. Chem.* **292**, 14695–14703 (2017).

23. V. F. Reichle, S. Kaiser, M. Heiss, F. Hagelskamp, K. Borland, S. Kellner, Surpassing limits of static RNA modification analysis with dynamic NAIL-MS. *Methods* **156**, 91–101 (2019).

24. J. E. Carette, M. Raaben, A. C. Wong, A. S. Herbert, G. Obernosterer, N. Mulherkar, A. I. Kuehne, P. J. Kranzusch, A. M. Griffin, G. Ruthel, P. D. Cin, J. M. Dye, S. P. Whelan, K. Chandran, T. R. Brummelkamp, Ebola virus entry requires the cholesterol transporter Niemann–Pick C1. *Nature* **477**, 340–343 (2011).

25. W. C. Clark, M. E. Evans, D. Dominissini, G. Zheng, T. Pan, tRNA base methylation identification and quantification via high-throughput sequencing. *RNA* **22**, 1771–1784 (2016).

26. R. Hauenschild, L. Tserovski, K. Schmid, K. Thüring, M.-L. Winz, S. Sharma, K.-D. Entian, L. Wacheul, D. L. J. Lafontaine, J. Anderson, J. Alfonzo, A. Hildebrandt, A. Jäschke, Y. Motorin, M. Helm, The reverse transcription signature of N-1-methyladenosine in RNA-Seq is sequence dependent. *Nucleic Acids Res.* **43**, 9950–9964 (2015).

27. G. Zheng, Y. Qin, W. C. Clark, Q. Dai, C. Yi, C. He, A. M. Lambowitz, T. Pan, Efficient and quantitative high-throughput tRNA sequencing. *Nat. Methods* **12**, 835–837 (2015).

28. P. Fechter, J. Rudinger, R. Giegé, A. Théobald-Dietrich, Ribozyme processed tRNA transcripts with unfriendly internal promoter for T7 RNA polymerase: Production and activity. *FEBS Lett.* **436**, 99–103 (1998).

29. N. T. Ingolia, S. Ghaemmaghami, J. R. S. Newman, J. S. Weissman, Genome-wide analysis in vivo of translation with nucleotide resolution using ribosome profiling. *Science* **324**, 218–223 (2009).

30. H. J. Chou, E. Donnard, H. T. Gustafsson, M. Garber, O. J. Rando, Transcriptome-wide analysis of roles for tRNA modifications in translational regulation. *Mol. Cell* **68**, 978–992.e4 (2017).

31. M. K. Thompson, M. F. Rojas-Duran, P. Gangaramani, W. V. Gilbert, The ribosomal protein Asc1/RACK1 is required for efficient translation of short mRNAs. *eLife* **5**, e11154 (2016).

32. B. Zinshteyn, M. F. Rojas-Duran, W. V. Gilbert, Translation initiation factor eIF4G1 preferentially binds yeast transcript leaders containing conserved oligo-uridine motifs. *RNA* **23**, 1365–1375 (2017).

33. D. D. Nedialkova, S. A. Leidel, Optimization of codon translation rates via tRNA modifications maintains proteome integrity. *Cell* **161**, 1606–1618 (2015).

34. M. Pereira, S. Francisco, A. S. Varanda, M. Santos, M. A. S. Santos, A. R. Soares, Impact of tRNA modifications and tRNA-modifying enzymes on proteostasis and human disease. *Int. J. Mol. Sci.* **19**, 3738 (2018).

35. A. Noma, S. Yi, T. Katoh, Y. Takai, T. Suzuki, T. Suzuki, Actin-binding protein ABP140 is a methyltransferase for 3-methylcytidine at position 32 of tRNAs in Saccharomyces cerevisiae. *RNA* **17**, 1111–1119 (2011).

36. S. D'Silva, S. J. Haider, E. M. Phizicky, A domain of the actin binding protein Abp140 is the yeast methyltransferase responsible for 3-methylcytidine modification in the tRNA anti-codon loop. *RNA* **17**, 1100–1110 (2011).

37. M. L. Gatza, G. O. Silva, J. S. Parker, C. Fan, C. M. Perou, An integrated genomics approach identifies drivers of proliferation in luminal subtype human breast cancer. *Nat. Genet.* **46**, 1051–1059 (2014).

38. A. G. Torres, E. Batlle, L. Ribas de Pouplana, Role of tRNA modifications in human diseases. *Trends Mol. Med.* **20**, 306–314 (2014).

39. S. Scheer, S. Ackloo, T. S. Medina, M. Schapira, F. Li, J. A. Ward, A. M. Lewis, J. P. Northrop, P. L. Richardson, H. Ü. Kaniskan, Y. Shen, J. Liu, D. Smil, D. McLeod, C. A. Zepeda-Velazquez, M. Luo, J. Jin, D. Barsyte-Lovejoy, K. V. M. Huber, D. D. De Carvalho, M. Vedadi, C. Zaph, P. J. Brown, C. H. Arrowsmith, A chemical biology toolbox to study protein methyltransferases and epigenetic signaling. *Nat. Commun.* **10**, 19 (2019).

40. P. Wirapati, C. Sotiriou, S. Kunkel, P. Farmer, S. Pradervand, B. Haibe-Kains, C. Desmedt, M. Ignatiadis, T. Sengstag, F. Schütz, D. R. Goldstein, M. Piccart, M. Delorenzi, Meta-analysis of gene expression profiles in breast cancer: Toward a unified understanding of breast cancer subtyping and prognosis signatures. *Breast Cancer Res.* **10**, R65 (2008).

41. X.-L. Tan, A. M. Moyer, B. L. Fridley, D. J. Schaid, N. Niu, A. J. Batzler, G. D. Jenkins, R. P. Abo, L. Li, J. M. Cunningham, Z. Sun, P. Yang, L. Wang, Genetic variation predicting cisplatin cytotoxicity associated with overall survival in lung cancer patients receiving platinum-based chemotherapy. *Clin. Cancer Res.* **17**, 5801–5811 (2011).

42. F. A. Ran, P. D. Hsu, C. Y. Lin, J. S. Gootenberg, S. Konermann, A. E. Trevino, D. A. Scott, A. Inoue, S. Matoba, Y. Zhang, F. Zhang, Double nicking by RNA-guided CRISPR cas9 for enhanced genome editing specificity. *Cell* **154**, 1380–1389 (2013).

43. C. B. Mulholland, M. Smets, E. Schmidtmann, S. Leidescher, Y. Markaki, M. Hofweber, W. Qin, M. Manzo, E. Kremmer, K. Thanisch, C. Bauer, P. Rombaut, F. Herzog, H. Leonhardt, S. Bultmann, A modular open platform for systematic functional studies under physiological conditions. *Nucleic Acids Res.* **43**, e112 (2015).

44. B. Linder, A. V. Grozhik, A. O. Olarerin-George, C. Meydan, C. E. Mason, S. R. Jaffrey, Single-nucleotide-resolution mapping of m6A and m6Am throughout the transcriptome. *Nat. Methods* **12**, 767–772 (2015).

45. W. M. Cai, Y. H. Chionh, F. Hia, C. Gu, S. Kellner, M. E. McBee, C. S. Ng, Y. L. J. Pang, E. G. Prestwich, K. S. Lim, I. R. Babu, T. J. Begley, P. C. Dedon, A platform for discovery and quantification of modified ribonucleosides in RNA. *Methods Enzymol.* **560**, 29–71 (2015).

46. K. Borland, J. Diesend, T. Ito-Kureha, V. Heissmeyer, C. Hammann, A. H. Buck, S. Michalakis, S. Kellner, K. Borland, J. Diesend, T. Ito-Kureha, V. Heissmeyer, C. Hammann, A. H. Buck, S. Michalakis, S. Kellner, Production and application of stable isotope-labeled internal standards for RNA modification analysis. *Genes* **10**, 26 (2019).

47. N. T. Ingolia, L. F. Lareau, J. S. Weissman, Ribosome profiling of mouse embryonic stem cells reveals the complexity and dynamics of mammalian proteomes. *Cell* **147**, 789–802 (2011).

48. M. V. Gerashchenko, V. N. Gladyshev, Ribonuclease selection for ribosome profiling. *Nucleic Acids Res.* **45**, e6 (2017).

49. E. E. Heyer, H. Ozadam, E. P. Ricci, C. Cenik, M. J. Moore, An optimized kit-free method for making strand-specific deep sequencing libraries from RNA fragments. *Nucleic Acids Res.* **43**, e2 (2015).

50. A. Dobin, C. A. Davis, F. Schlesinger, J. Drenkow, C. Zaleski, S. Jha, P. Batut, M. Chaisson, T. R. Gingeras, STAR: Ultrafast universal RNA-seq aligner. *Bioinformatics* **29**, 15–21 (2013).

51. A. Rau, M. Lina Gallopin, G. Celeux, F. J. Zic, Gene expression data-based filtering for replicated high-throughput transcriptome sequencing experiments. 29, 2146–2152 (2013).

52. M. I. Love, W. Huber, S. Anders, Moderated estimation of fold change and dispersion for RNA-seq data with DESeq2. *Genome Biol.* **15**, 550 (2014).

53. H. Fuchs, V. Gailus-Durner, T. Adler, J. A. Aguilar-Pimentel, L. Becker, J. Calzada-Wack, P. Da Silva-Buttkus, F. Neff, A. Götz, W. Hans, S. M. Hölter, M. Horsch, G. Kastenmüller,

E. Kemter, C. Lengger, H. Maier, M. Matloka, G. Möller, B. Naton, C. Prehn, O. Puk, I. Rácz, B. Rathkolb, W. Römisch-Margl, J. Rozman, R. Wang-Sattler, A. Schrewe, C. Stöger, M. Tost, J. Adamski, B. Aigner, J. Beckers, H. Behrendt, D. H. Busch, I. Esposito, J. Graw, T. Illig, B. Ivandic, M. Klingenspor, T. Klopstock, E. Kremmer, M. Mempel, S. Neschen, M. Ollert, H. Schulz, K. Suhre, E. Wolf, W. Wurst, A. Zimmer, M. Hrabě de Angelis, Mouse phenotyping. *Methods* **53**, 120–135 (2011).

54. B. Rathkolb, W. Hans, C. Prehn, H. Fuchs, V. Gailus-Durner, B. Aigner, J. Adamski, E. Wolf, M. Hrabě de Angelis, Clinical chemistry and other laboratory tests on mouse plasma or serum. *Curr. Protoc. Mouse Biol.* **3**, 69–100 (2013).

55. Z. Tang, C. Li, B. Kang, G. Gao, C. Li, Z. Zhang, GEPIA: A web server for cancer and normal gene expression profiling and interactive analyses. *Nucleic Acids Res.* **45**, W98–W102 (2017).

56. J. Gao, B. A. Aksoy, U. Dogrusoz, G. Dresdner, B. Gross, S. O. Sumer, Y. Sun, A. Jacobsen, R. Sinha, E. Larsson, E. Cerami, C. Sander, N. Schultz, Integrative analysis of complex cancer genomics and clinical profiles using the cBioPortal. *Sci. Signal.* **6**, pl1 (2013).

57. E. Cerami, J. Gao, U. Dogrusoz, B. E. Gross, S. O. Sumer, B. A. Aksoy, A. Jacobsen, C. J. Byrne, M. L. Heuer, E. Larsson, Y. Antipin, B. Reva, A. P. Goldberg, C. Sander, N. Schultz, The cBio cancer genomics portal: An open platform for exploring multidimensional cancer genomics data. *Cancer Discov.* **2**, 401–404 (2012).

Author contributions: V.V.I., S.M.K., E.G., O.J.R., and R.S. designed the study and analyzed data. V.V.I. and R.S. wrote the manuscript with feedback from all authors. J.S.Y.H., Y.X.T., F.P.H.G., C.L.L., A.P., and E.G. performed shRNA screening and experiments with HepG2 cells. V.V.I. performed in vitro and cell culture experiments with help from P.R.L., M.V., and E.I. S.K. and S.M.K. performed LC/MS-MS experiments. X.B. and O.J.R. performed RNA-seq and ribosome profiling and corresponding data analysis. P.S. and S.B. generated KO mESCs and studied pluripotency. S.Lu. performed data analysis that was not part of the final manuscript but was essential for experiment design. S.M. generated the *Mettl6* cohort for mouse phenotyping tests. R.G., B.R., A.A.-P., A.S.-M., T.K.-R., and J.C.-W. performed mouse phenotyping tests and analyzed the data. S.Le., H.F., V.G.-D., and M.H.d.A. supervised the mouse project and conceived the phenotypic test pipeline. **Competing interests:** The authors declare that they have no competing interests. **Data and materials availability:** Ribosome footprinting and corresponding RNA-seq data (Fig. 4) have been deposited to Gene Expression Omnibus under accession number GSE144866. RNA-seq data used for Fig. 4B have been deposited to ArrayExpress under ID no. ID E-MTAB-8872. All other data needed to evaluate the conclusions in the paper are present in the paper and/or the Supplementary Materials. Additional data related to this paper may be requested from the authors. Correspondence and requests for materials should be addressed to R.S. (robert.schneider@helmholtz-muenchen.de).

Citation: V. V. Ignatova, S. Kaiser, J. S. Y. Ho, X. Bing, P. Stolz, Y. X. Tan, C. L. Lee, F. P. H. Gay, P. R. Lastres, R. Gerlini, B. Rathkolb, A. Aguilar-Pimentel, A. Sanz-Moreno, T. Klein-Rodewald, J. Calzada-Wack, E. Ibragimov, M. Valenta, S. Lukauskas, A. Pavesi, S. Marschall, S. Leuchtenberger, H. Fuchs, V. Gailus-Durner, M. H. de Angelis, S. Bultmann, O. J. Rando, E. Guccione, S. M. Kellner, R. Schneider, METTL6 is a tRNA m^{3}C methyltransferase that regulates pluripotency and tumor cell growth. *Sci. Adv.* **6**, eaaz4551 (2020).

Science Advances

METTL6 is a tRNA m^{3}C methyltransferase that regulates pluripotency and tumor cell growth

Valentina V. Ignatova, Steffen Kaiser, Jessica Sook Yuin Ho, Xinyang Bing, Paul Stolz, Ying Xim Tan, Chee Leng Lee, Florence Pik Hoon Gay, Palma Rico Lastres, Raffaele Gerlini, Birgit Rathkolb, Antonio Aguilar-Pimentel, Adrián Sanz-Moreno, Tanja Klein-Rodewald, Julia Calzada-Wack, Emil Ibragimov, Magdalena Valenta, Saulius Lukauskas, Andrea Pavesi, Susan Marschall, Stefanie Leuchtenberger, Helmut Fuchs, Valerie Gailus-Durner, Martin Hrabe de Angelis, Sebastian Bultmann, Oliver J. Rando, Ernesto Guccione, Stefanie M. Kellner and Robert Schneider

ARTICLE TOOLS	http://advances.sciencemag.org/content/6/35/eaaz4551
SUPPLEMENTARY MATERIALS	http://advances.sciencemag.org/content/suppl/2020/08/24/6.35.eaaz4551.DC1
REFERENCES	This article cites 56 articles, 10 of which you can access for free http://advances.sciencemag.org/content/6/35/eaaz4551#BIBL
PERMISSIONS	http://www.sciencemag.org/help/reprints-and-permissions

Use of this article is subject to the Terms of Service